Micaela Tavares Oliveira

Electrochemical pH monitoring in cell culture systems

Micaela Tavares Oliveira

UMinho | 2021

Universidade do Minho
Escola de Ciências

Micaela Tavares Oliveira

Electrochemical pH monitoring in cell culture systems

julho 2021

Universidade do Minho
Escola de Ciências

Micaela Tavares Oliveira

Electrochemical pH monitoring in cell culture systems

Master thesis

Master in Biophysics and Bionanosystems

Work developed under the supervision of

Dr. Alar Ainla

Prof. Dr. Elisabete Maria dos Santos Castanheira Coutinho

julho 2021

DIREITOS DE AUTOR E CONDIÇÕES DE UTILIZAÇÃO DO TRABALHO POR TERCEIROS

Acknowledgements

I would like to start by thanking my supervisor Alar Ainla. Since he became my supervisor, he stepped in and guided me through this journey. I became his "minion", following him around and asking all the questions that came across my head. For the endless debates, scientific puzzles, tricky questions and for teaching me to see the realm of science from a different perspective. All the MATLAB scripts for the statistical analysis as well as the electronic devices used were produced by him , allowing me to finish the work started. For all the dedication, mentoring and support you deserve a special thank you.

To Lorena Diéguez, thank you for having accepted me in your research group and making me always feel welcomed and for helping me with all the adversities that came across throughout this project.

To Professor Elisabete Coutinho, for all the help and orientation given to make the completion of this dissertation possible.

To Medical devices research group for receiving me and integrating me in your group. And a special thanks to Alexandra Teixeira for always helping in the lab every time I felt lost.

To my friends from my master, who join me in this journey in INL I thank you, specially Patrícia Rodrigues, Marisol Dias, Ânia Micaelo, for sharing the good and the bad moments, always with a smile.

To my little "minion" Ana Martins. You gave me back my excitement for science during this hard journey, always making the work place a fun environment.

And finally, I would like to thank my family. My parents, Manuela and Ângelo, because without you and all your sacrifices, I wouldn't be here today finishing my thesis. And also, a massive thanks to my sister, Tânia, for all the encouragement and support throughout this rollercoaster we call life.

STATEMENT OF INTEGRITY

I hereby declare having conducted this academic work with integrity. I confirm that I have not used plagiarism or any form of undue use of information or falsification of results along the process leading to its elaboration.

I further declare that I have fully acknowledged the Code of Ethical Conduct of the University of Minho.

Monotorização eletroquímica do pH em sistemas de culturas celulares

Resumo

O cancro é umas das doenças com maior taxa de mortalidade em países desenvolvidos. Em ordem a desenvolver estratégias terapêuticas para a prevenção do seu crescimento e propagação, uma compreensão detalhada do tecido cancerígeno e a atividade metabólica das células é requerida. Todavia, a monotorização *in vivo* do cancro em humanos é desafiante e os modelos animais oferecem uma exatidão limitada na reprodução desta doença. Por esse motivo, modelos *in vitro organ-on-a-chip* melhorados, que mimetizam as suas características são necessitados urgentemente.

O microambiente do cancro tem uma grande influência no seu comportamento, onde o pH e a acidificação extracelular são alguns dos parâmetros essenciais. Por esta razão, nesta tese nós desenvolvemos um sistema de deteção para a monitorização do pH, em tempo real, em modelos cancerígenos *on-a-chip*. A nossa abordagem baseia-se na deteção eletroquímica potenciométrica, na qual variações na concentração de protões são detetadas através da medição das diferenças de potencial entre um elétrodo de óxido de irídio e um elétrodo de referência de cloreto de prata. Os testes de otimização têm sido realizados com o objetivo de obter um sistema de medição para monitorização em culturas celulares por longos períodos de tempo. Primeiramente, o sistema foi testado em modelos de cultura celular em 2D, uma placa de 6 poços. Este passo intermediário funciona para comprovar que o sistema otimizado poderá ser utilizado com sucesso em culturas celulares, antes de prosseguirmos com a integração e os testes no modelo 3D desenvolvido. Por outro lado, também potencia o desenvolvimento de uma nova aplicação para este sistema de medição, como por exemplo um sistema de monitorização do pH durante testes realizados em modelos em 2D, como em testes para o desenvolvimento de fármacos. Deste modo, nós apresentamos o progresso da otimização de um modelo microfluídico para o cancro, integrado com um sensor de pH. Tal sistema pode ser útil como plataformas para a pesquisa do cancro e, eventualmente, traçar o caminho como um instrumento clínico para determinar a melhor opção de tratamento personalizado.

Palavras-chave: cancro, cultura 3D, eletroquímica, pH, sensores

Electrochemical pH monitoring in cell culture systems

Abstract

Cancer is one of the diseases with the highest mortality rates in developed countries. In order to develop therapeutic strategies for the prevention of its growth and spreading, detailed understanding of the cancerous tissue and metabolic activity of cells is required. However, *in vivo* monitoring of cancer in humans is challenging and animal models can only offer limited accuracy in reproducing this disease. Therefore, improved *in vitro* cancer on-a-chip models, mimicking its features are urgently needed. It is known that cancer microenvironment has a high influence on its behaviour, where local pH and extracellular acidification are one of the essential parameters. Hence, in this thesis we have developed a sensing system for monitoring pH in real time in cancer models on-a-chip. Our approach is based on electrochemical potentiometric sensing, in which changes in the concentration of protons are detected by measuring potential differences between an IrOx based electrode and a Ag/AgCl reference electrode. Optimization testing has been directed towards achieving a stable sensing system for long term cell culturing. This system has been first tested in a 2D cell culture system, a 6 multiwell plate. This middle step provides a proof of concept that the sensing system can be successfully applied to cell culture systems before undergoing further developments to integrated it in the 3D chip. On the other hand, it also allows for the development of new application for such system, such as pH monitoring during different assays involving multiwell culturing, for instance for drug testing applications. Hereby, we present an ongoing development and optimization of a microfluidic system for cancer on a chip model with the integrated sensing capabilities. Such system can be useful as cancer research platforms and eventually pave the way also to clinical tools for determining the best personalized treatment options.

Keywords: 3D culture, cancer, electrochemistry, pH, sensors

Contents

List of Figures

List of Supplementary Figures

List of Tables

List of Supplementary Tables

List of Abbreviations

ADC	Analog-to-digital converter
AEIROF	Anodically Electrodeposited Iridium Oxide Films
ANG-1	Angiopoietin-1
BC	Bone-on-a-chip
CTC	Circulating tumour celll
CV	Cyclic voltammetry
DMEM	Dulbecco's Modified Eagle's Medium
EC	Endothelial cells
ECM	Extracellular matrix
FET	Field-Effect Transistor
FRET	Förster Resonance Energy Transfer
FSB	Fetal Bovine Serum
HK	Hexokinase
HUVEC	Human Umbilical Vein Endothelial Cells
IC_{50}	Half maximal inhibitory concentration
ICT	Intramolecular Charge Transfer
IGFET	Insulated Gate Field Effect Transistor
IL-2	Interleukin-2
ISE	Ion Selective Electrodes
ISFET	Ion Sensitive Field Effect Transistor
IUPAC	International Union of Pure and Applied Chemistry
JFET	Junction Field Effect Transistor
LAPS	Light Addressable Potentiometric Sensor
MCT	Monocarboxylate transporters
MEA	Microelectrode array
MEMS	Microelectromechanical systems
MOC	Metastasis-on-a-chip
MOSFET	Metal Oxide Semiconductor Field Effect Transistor
MRI	Magnetic Resonance Imaging
NC	Nitrocellulose
NIR	Near-Infrared
OOAC	Organ-on-a-chip
OXPHOS	Oxidative Phosphorylation
PAEC	Porcine Aortic Endothelial Cells
PBS	Phosphate-buffered saline
PDMS	Poly(dimethysiloxane)
PEG	Polyethylene glycol
PEI	Poly(ethyleneimine)
PET	Positron Emission Topography
PFK	Phosphofructokinase
pHe	pH extracellular

pHi	pH intracellular
PHI	Phosphohexose Isomerase
PK	Pyruvate Kinase
PMMA	Poly (methyl methacrylate)
RE	Reference electrode
SE	Sensing electrode
TCA	Tricarboxylic acid cycle
TMZ	Temozolomide
VEGF	Vascular endothelial growth factor
VMT	Vascularized Microtumours

1. Introduction

1.1. Current challenges in drug delivery and development

For the last decades, the pharmaceutical industry has faced several hurdles in the market approval of new drugs, with a success rate of only about 10%. After the target compound is synthesised, its efficiency is assessed in three phases: *in vitro* experiments in 2D cell culture models (I), *in vivo* experiments in animal models (II), and clinical trials in humans (III) (1). These different stages serve the purpose of evaluating toxicity, absorption, distribution, metabolism and efficacy of drug compounds. Generally, the drugs under development fail in late stages, commonly in the last phase, which increases the costs for pharmaceutical companies (1).

Though conventionally practised, 2D cell culture is one of the main causes attributed to the failure in the development of new drugs. Its monolayer growing format on plastic surfaces limits the surroundings of cells and, consequently, their interaction with each other and with their microenvironment (1). The lack of an extracellular matrix affects cell signalling, influencing deeply cells' expression profile and its differentiation, preventing 2D models from accurately reproduce *in vivo* physiological conditions (2). Moreover, animals do not always represent reliable models for human tissue representation and the ethical issues surrounding their use in research remain entangled in controversy. Hence, it has become imperative to establish new methodologies that would function as a bridge between traditional 2D cell culture techniques and *in vivo* testing. *In silico* models have also been proposed as a valid option, however, 3D cell culture has proven to be the most promising solution to this pressing matter as an alternative to the conventional *in vitro* and *in vivo* animal models or even as a replacement of these.

1.2. Traditional *in vitro* cell culture systems

Traditional 2D culture models include petri dishes, flasks and multiwell plates. These methods have been consistently used in drug screening due to their simple handling, low cost, high reproducibility and accessibility, and easiness for imaging (3). They are, however, oversimplified models, where interactions between cells and the extracellular matrix are limited and do not represent an accurate translation of the *in vivo* tissue's environment. Cells attached to rigid plastic surfaces possess polarized growth and their access to nutrients and oxygen is increased, precluding the generation of concentration gradients (4). Concentration gradients exist naturally in the physiological systems for different parameters, like oxygen, pH, nutrients, and other metabolites. Those are mainly produced because of the different distances of cells from blood vessels. Gradients are fundamental in biological systems, for example in processes of

morphogenesis and angiogenesis. In the tumour microenvironment oxygen gradients are prevalent, originated from different layers of proliferating cells or cells in quiescent stage or hypoxic, and altering cells resistance to drugs. Furthermore, the absence of a proper extracellular matrix (ECM) influences greatly the drug response given by these models. ECM is formed by a plethora of components, such as collagens, fibronectin, proteoglycans, and growth factors such as vascular endothelial growth factor (VEGF), affecting several cell behaviours, such as proliferation, migration, differentiation, signalling pathways, and cytoskeletal organization (2). For example, ECM controls cells signalling by indirectly affecting the diffusion of soluble molecules or directly through the bonding of specific motifs of peptides of ECM to integrins present in cells membranes. Likewise, the physical properties of ECM, which are correlated to its chemical composition, induce different phenotypes in cells by altering genetic expression. Cells can detect changes in matrix rigidity and convert those mechanical signals into chemical responses, as it happens with the Rho/ROCK signalling pathway (4).

Additionally, the presence of stromal cells also represents a major necessity for completion of *in vitro* models. *In vivo*, cells are also in contact with connective tissue, where mesenchymal cells are embedded, such as fibroblasts and glial cells for the neuronal tissues, as it is with the immune system. These cells can play a part in processes like angiogenesis and vasculogenesis. These have been showed for example, by Sudong Kim and colleagues when they developed a microfluidic chip to create 3D perfusable microvessels through processes of angiogenesis and vasculogenesis. Their microfluidic chip was composed of five parallel channels, where the central channel contained the endothelial cells and the ECM, which would originate the blood vessels; the central channel was enclosed by two fluidic channels, which are themselves enclosed by two other channels where the stroma cells grow. The vessels were formed by culturing HUVECs (Human Umbilical Vein Endothelial Cells) cells in a fibrin matrix, supported by the pro-angiogenic growth factors secreted by the human lung fibroblasts. They concluded that to form perfusable interconnected networks of vessels, endothelial cells needed to be co-cultured with lung fibroblasts, but separately in different channels, to generate a gradient. The 3D structure of the formed vessels was studied along with the presence of biomarkers in healthy vessels, such as the existence of a lumen, cells junctions, a basement membrane, followed by the determination of the perfusion and permeability values. The flow effect upon the vasculature was also tested, at the cytoskeleton level along with the synthesis of NO (nitric oxide) from ECs (Endothelial cells) and the influence of other cells to the microenvironment, like the cancer cell line U87MG, where they verified the formation of aberrant microvascular networks (5).

As an alternative to 2D models, 3D cell culture systems have emerged. These can be split into two categories: (1) anchorage-independent cultures and (2) scaffold cell cultures (2). Spheroids or "multicellular spheroids" are examples of scaffold free 3D cultures, consisting of well-rounded cell aggregations formed of multiple single cells (epithelial, mesenchymal, endothelial, etc) (6). These spheroid structures create gradients of oxygen, pH and nutrients, resulting in heterogenic cells populations, with hypoxic layers and proliferating layers (6). These cell structures are formed by preventing the adhesion of cells to the bottom of wells or flasks, forcing them to aggregate, through different methods, such as the hanging drop technique. On the other hand, 3D cell cultures can be formed by adding cells inside artificial or natural scaffolds, providing a rigid structure as support and where cells can develop ECM and cell-cell interactions, mimicking *in vivo* systems. Matrigel is a natural scaffold commonly used in 3D cell culture, however, since it is obtained from animals it creates a variability associated in terms of stiffness and composition, affecting reproducibility (2). As an alternative, there are synthetic scaffolds made of materials such as polyethylene glycol (PEG), poly(lactide-co-glycolide) (PLG) and polylactic acid (PLA) (2).

2D methodologies are still conventionally used for cancer research and are essential for the development of new chemotherapies. Nonetheless, great efforts are being put to substitute 2D cell culture techniques with these 3D cell culture models to avoid the inaccuracy that comes with the lack of complexity of 2D models. This is particularly important for drug screening experiments, where the drug resistance phenomenon as been proven to be associated with the multiplexity of the culture models.

1.3. Organ-on-a-chip

Traditional 3D cell culture models are still seen as insufficient due to the lack of vasculature, control of gradients and a continuous supply of medium (7). The significant arise of microfluidics changed radically the *in vitro* cell culture techniques and brought a panoply of new of 3D cell culture systems.

Microfluidics is a field of science and technology that focuses on the manipulation of small amounts of liquids inside channels with microscale dimension (10 to 100 micrometers) (8). Microelectronics was one of the contributions to the development of microfluidic systems, through the adaptation and application of the same fabrication techniques (photolithography) that were already used to produce microelectromechanical systems (MEMS) (8). Unlike MEMS, most of the microfluidic systems have been constructed using poly(dimethylsiloxane) (PDMS). An elastomer, distinguished for its optical transparency, flexibility and biocompatibility (8).

Advancements in microfluidics allowed different types of cells in a co-culture to be spatially organized (cell patterning), like it happens *in vivo* tissues as well as the development and control of gradients and the flow through the channels (7).

The introduction of microfluidics in 3D cell culture created models such as organ-on-a-chips (OoaC). Organ-on-a-chip is a microfluidic system for cell culture purposes, that is continuously perfused through micrometre channels, which provide medium renewal and removal of the cell waste (9). These systems can provide the control of key parameters, making the cellular environment closer to what occurs *in vivo*. Fluid shear stress, concentration gradients, mechanical stress, and cell patterning are some of the most relevant features to replicate (10). The OoaC systems are typically formed by three major components: microfluidics, cell culture and sensing systems.

OoaC have been used to mimic several organs and tissues, such as lung-on-chip (11), liver-on-chip (12); heart on-chip (13), bile-duct on chip (14); gut-on-chip (15), brain-on-chip and even placenta-on-chip (16) has been reported. More complex systems have been developed, containing more than one type of organ in the same chip, which brings the advantage of analysing the effect of the same drug in multiple tissues simultaneously, for example (17). Organs-on-chip have also been used to study different diseases which could eventually lead to new therapeutical strategies.

Dongeun Huh et al. reported a lung-on-a-chip model to study the formation of pulmonary edema in human lungs. The accumulation of intravascular fluid inside the alveolus could be induced by the prolonged use of a drug for treatment of malignant melanoma and metastatic renal cell carcionoma, interleukin-2 (IL-2). The researchers were able to design and develop a lung-on-a-chip microdevice that recreated the fluid accumulation and the fibrin deposition that comes with it. They discovered that breathing motions aggravated the toxic effects of IL-2 by increasing the permeability of epithelial and endothelial barriers and suggested GSK2193874 (GlaxoSmithKline), an inhibitor of TRPV4 channels, known for increasing permeability, and Ang-1 (angiopoietin-1) as possible therapeutic agents to supress vascular leakages. These results were also confirmed by *ex vivo* culture, using a rat's lung. However, the study of the effect of mechanical movements during breathing did not included proper quantification, leaving the pressure values that exacerbated the leakage unknown (18).

OoaC have also been repeatedly applied for drug screening. Carlota Oleaga et al, presented multi-organ human chip containing cardiac, muscular, hepatic, and neuronal tissues with the purpose to evaluate toxicity of five different pharmaceutical compounds over a 14-day period. This four-organ system with a

systemic medium circulation was able to mimic *in vivo* human tissues and determine quantitively the response to different drugs through electrical, mechanical, and metabolic measurements (19).

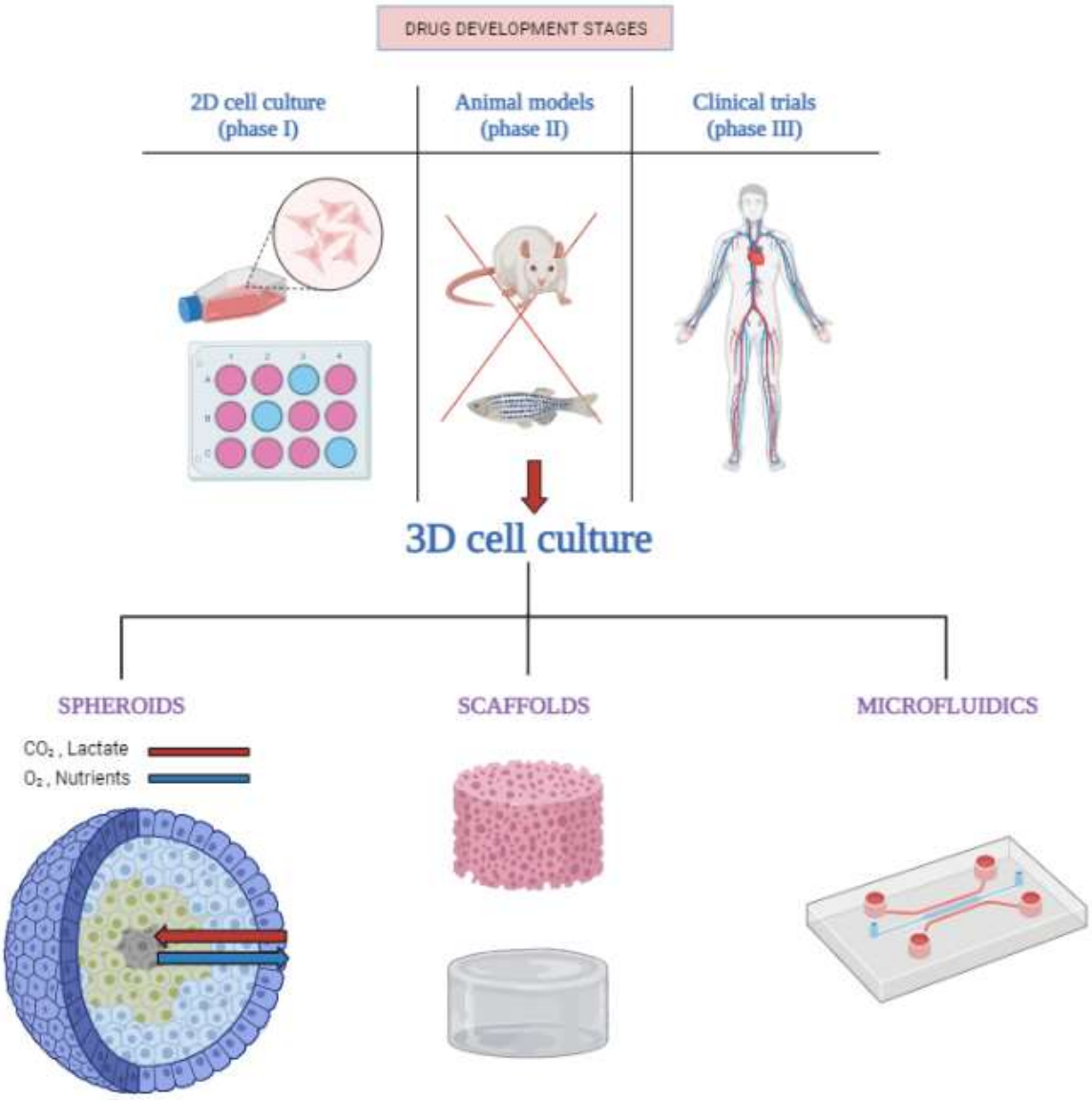

Figure 1. Schematic representation of conventional stages of drug development and the new in vitro 3D culture systems developed as an alternative to the traditional 2D culture systems (created in biorender)

1.4. Biomimetic 3D Cancer Models

Cancer is one of the diseases with the highest mortality rate in developed countries. Its early diagnosis is pivotal to prevent its spreading and ensure a successful treatment. Cancer research has often been conducted using conventional methods, such as 2D cell culture. However, the conditions presented in 2D cultures are not ideal for cancer studies. Cells are attached to rigid surfaces, with no 3D structure, with an excessive supply of media and a limited ECM matrix. This deviates from the oxygen gradients and the ECM matrix composition typically present in tumour environments (4). Such differences can be observed, when comparing the results obtained from the 2D cell culture assays and *in vivo* studies (20). Thus, it has become evident the need to use the latest 3D cell culture techniques for the research of cancer and tumour progression.

Many cancer OoaC devices have been developed with the purpose of improving the current *in vitro* systems available for cancer research and step forward the personalized platforms based on cancerous cells from each patient. Agua Sobrino et al, presented a platform containing vascularized microtumours (VMT) to investigate the close interaction between tumour masses and vessels, and how these systems respond to common anti-cancer drugs. The microfluidic chip consisted of three tissue chambers connected to two loading openings and two adjacent channels where medium flows from the reservoirs towards the outlets. First the vasculature formation was induced by the presence of endothelial cells, stromal cells and ECM elements. Once the vasculature was built, the human colorectal cancer cell line HCT116 was introduced inside those chambers to form structures around and within the vessels constructs. Several other cancer cell lines were studied, gaining the understanding of different morphologic and chemical composition specifications for each of the tumours. Drug responses were analysed regarding their effect to the metabolism of cancer cells and the effect to the vasculature, opening the therapeutic targets to agents that disrupt tumours microvessels. The investigators also observed differences in the IC_{50} (half maximal inhibitory concentration) doses of drugs between 2D and the 3D cultures they developed, as expected, emphasizing the importance of complexity of *in vitro* models. A downside of this platform would be the lack of immune cells in the microenvironment, and posterior studies of their effect in the overall system (21).

However, about 90% of cancer deaths are owned to the spreading of cancer cells from the primary tumour across the entire organism, leading to the formation of metastatic tissue. Metastasis corresponds to a sequence of processes that can be summarized as following: invasion of the surrounding tissues (A) ECM degradation and separation from the primary tumour (B) entry into the circulatory system (intravasation)

(C) migration from the blood circulatory system (extravasation) into the surrounding tissue (D) cell proliferation and metastasis formation. The study of metabolic alterations, that occur during the metastatic development, is crucial to understand how cells can disseminate across different sites after they leave the primary tumour and survive. Aside from that, ECM has a very significant role in tumorigenesis that is beyond of providing a solid structure. Through the means of biochemical and mechanical signalling, it can trigger cellular response mechanisms and advance tumour progression On that line of thought, the 2D models that have been used to study the migration of cancerous cells for example have become insufficient, enhancing the urgency to create "metastasis-on-a-chip" (MoC) models.

Approximately, 70% of breast cancers form metastatic clusters in bone tissue. With the purpose to elaborate a realistic *in vitro* model of bone tissue as a target of metastatic cells, Sijie Hao and team, developed a mineralized bone-on-a-chip (BC) model, co-cultured with breast cancer cell lines. This system consisted of a bottom chamber for osteoblastic tissue growth, followed by a top medium reservoir, with a separation of dialysis membrane, and all settled on a glass cover slip. After a careful analysis of different versions of BCs, the team chose a bone-on-a-chip model with a nitrocellulose (NC) membrane and a cell culture chamber with a 2 mm height. In NC-BC osteoblastic tissue grew, matured, and formed a mineralized and collagen rich matrix for a month period. After establishing an ideal BC model, they proceeded to co-culture the bone tissue, with two breast cancer cell lines, MDA-MB-231, and a metastasis supressed cell line, MDA-MB-231-BRMS1. 88.5% of the first cell line formed micrometastasis, while for the suppressed cell line only 61.4% formed micrometastasis, being observed in fluorescence microscopy loose cells, not embedded in the osteoblastic tissue (22).

Aleksander Skardal et al. also reported a MoC, with an image tracking of cancer cells in order to visualize tumour progression across a circulatory system. This chip connected two main chambers forming the gut and the liver constructs, built by the photopolymerization of hydrogel encapsulating the cells. The flow system allowed the primary foci of carcinoma cells formed in the gut, to disseminate and spread to the liver construct. Two cell lines of fluorescently labelled colon carcinoma cells with different metastatic tendencies were used. The more metastatic cell line (HCT-116) proliferated, entered the circulating system, and formed metastasis in the liver construct, while the less metastatic cell line proliferated less and did not disseminate from the primary tumour. ZO-1, B catherin and vinculin (markers associated with epithelial phenotype) were only expressed in 10-40% of the HCT-116 cells, while MMP-9, N-cadherin and PCNA (markers associated with a mesenchymal phenotype) were expressed in 90% of the HCT-116

cells. Such results are contradictory with the ones obtained in 2D models, in which the HCT-116 expresses the epithelial markers, underlining once again the differences between these two types of *in vitro* models. The mechanical properties of the hydrogel were also in the scope of the research, having in mind the importance of the microenviroment for tumorigenesis. Thus, they concluded that, the change in the stiffness of hydrogels, by altering the concentration of crosslinking agents, can promote the archetypal malignant behaviours of metastatic cells. Hereby, the results showed that soft tumours constructs, and a stiff microenvironment resulted in cells migration. At last, this model was used for drug testing, demonstrating the effects that drugs, such as Marismastat, have on the development of metastasis (23).

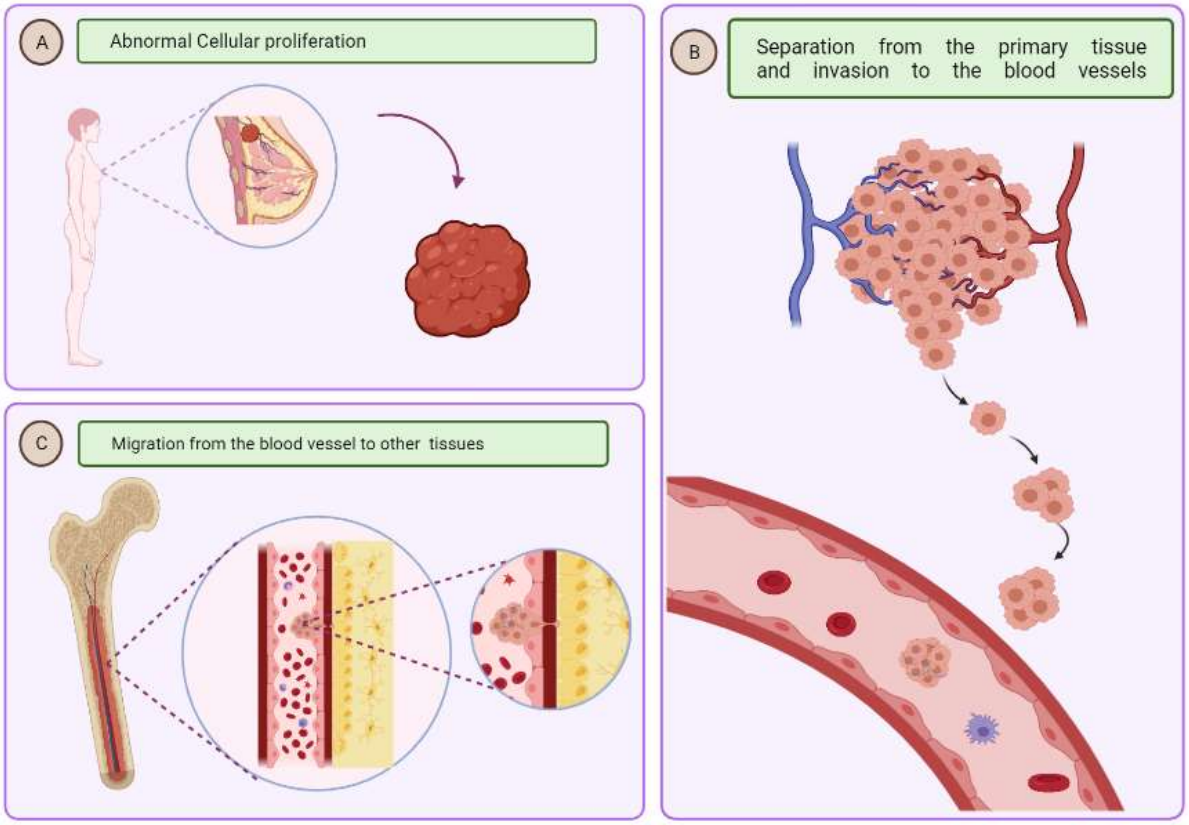

Figure 2. Schematic representation of the different phases of the metastasis of the cells: Uncontrolled cell proliferation and formation of primary tumour (A), ECM degradation, separation from the primary tumour and entry into the circulatory system (intravasation) (B), migration from the blood circulatory system (extravasation) into the surrounding tissue, cell proliferation and metastasis formation (C) (created in biorender).

1.5. pH sensing for cancer

1.5.1. pH definition and biological importance

pH determines the acidity or the alkalinity of solutions. In 1909, Sørensen provided a mathematical definition for pH, according to which the pH is given by the negative logarithm of the hydrogen ion concentration (24):

$$\text{pH} = -\log_{10}[H^+] \qquad \text{Equation (1)}$$

This initial definition was later modified by Sørensen and Linderstrøm-Lang, by adding an activity factor, which also considers the interaction between the hydrogen ions and other electrolytes present in the solution (24):

$$\text{pH} = -\log_{10} a[H^+] \qquad \text{Equation (2)}$$

The pH is dependent of the ionic strength of a solution. Thus, the activity of each electroactive species in a solution, including the hydrogen ions, results from the multiplication of its concentration, c, by a correction factor γ (24):

$$a = c\ \gamma\ (3) \qquad \text{Equation (3)}$$

The pH is an important parameter for the homeostasis of organisms. Enzymatic activities that participate in several chemical reactions are pH dependent, making its regulation of extreme relevance for the function of life. Phosphofructokinase is an example of an enzyme that stops working under acidic conditions (24). On the other hand, blood pH values vary between 7.35 and 7.45, and this range is kept through the action of buffers such as hemoglobin, albumin and bicarbonate reabsorption in the renal tubules (25)(26). A slight change in such values may lead to acidosis for example, causing pathologies.

1.5.2. Cancer metabolism

The origin of cancer is mainly attributed to mutations in oncogenes and tumour suppressors and its effect in the metabolic activities of cells. The loss of tumour suppressor proteins is an important hallmark of cancer. p53 is one of the most well studied tumour suppressors and approximately 50% of the cancers are associated with mutations in this gene. During cellular division, p53 stops its progress, if DNA is damaged, preventing the errors to be continuously replicated (27).

Regarding the energetic demands of cancer cells, several types of cancer cells exhibit the so called "Warburg effect". This hallmark in cancer metabolism consists of the preferential pathway of aerobic

glycolysis (even under anaerobic conditions) to sustain their energetic needs, as a replacement of mitochondrial oxidation (27). The origin of this phenomena varies, and it used to be credit to abnormal mitochondrial functioning. Currently we know that the activation of oncogenes, as the signalling protein KRAS and the transcription factor MYC, loss of tumour suppressors, and up-regulation of the PI3K/AKT/mTOR pathway are the attributed causes to the Warburg effect (27)(28). Despite what was thought, the high glycolysis rates are not due to the need to fulfil the energetic requirements of cells, but to ensure the synthesis of biological precursors for other metabolic pathways needed for the cell proliferation. Besides tumour proliferation, it is hypothesized that the aerobic glycolysis is also one of the factors leading to the malignancy of tumours.

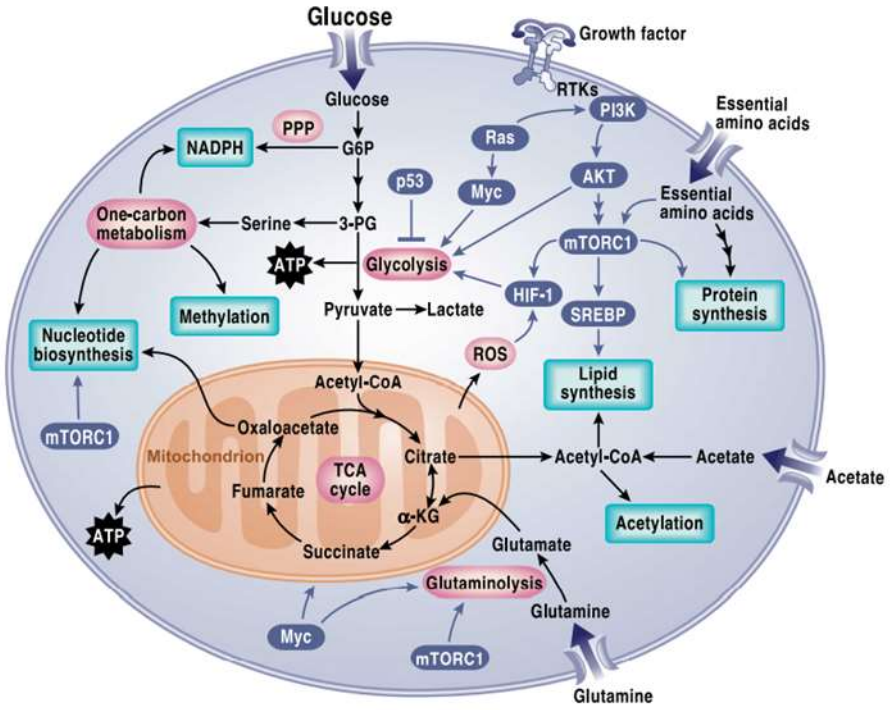

Figure 3. Schematic representation of the cancer cells metabolism from Ralph J. DeBerardinis et al (28)

Glycolysis has been linked to the Warburg effect and to the metastasis development, where some glycolytic genes have been shown to promote it, such as hexokinase (HK), pyruvate kinase (PK), phosphohexose isomerase (PHI) and phosphofructokinase (PFK) – enzymes that catalyse reactions in glycolysis. PI3K is an example of an oncogene which regulates the metabolism of glycolysis by up-regulating glycolytic genes such as PFK-1, PFK2 and HK1 (27).

TCA cycle produces several components that participate in multiple metabolic pathways in the cell. An upregulation of the TCA cycle is also a response from detached cells, such as CTC's (circulating tumour

cells), when glucose uptake is affected, to guarantee the ATP production, through the formation of NADH and $FADH_2$. The acetyl-CoA, used by TCA cycle in case of impaired glucose uptake is provided by fatty acid oxidation (FAO) (29). Other biosynthetic intermediates produced because of TCA cycle are also known to induce malignant properties present in tumour cells, like alpha-Ketoglutarate (αKG), which participates in epigenetic regulation, thus representing a potential source of modifications which may lead to tumour progression (30). On the other hand, the mutate form of the enzyme IDH (isocitrate dehydrogenase) present in the TCA cycle is responsible for the generation of oncometabolites, such as succinate. Together with the TCA cycle comes the OXPHOS (Oxidative Phosphorylation) pathway, which prevents death of detached cells by production of ATP. This pathway is upregulated only in detached cells, where surviving is the priority, while proliferating cancer cells have taken aerobic glycolysis as the metabolic route of choice (30).

Besides FOA, fatty acid synthase (FAS) is also up regulated in cancer cells for the production of some of cells building stones like lipidic membranes (29). Aminoacids such as methionine, asparagine, serine and glutamine play an important part in different phases of tumour progression. Glutamine can be converted in glutamate by glutaminase, which is a precursor for the glutathione cycle, an important antioxidant, especially useful in cells with high metabolic rates, like cancer cells. Redox balance is extremely relevant for metastasis, since high concentrations of reactive oxygen species (ROS) inhibit PKM2, affecting glycolysis. To assure this balance, pentose phosphate pathways is upregulated, especially in cells detached from the ECM, through the production of NADPH, a key element for the glutathione cycle (30).

These are just a few considerations regarding tumorigenesis and the metabolic changes cells must undergo to reach a malignant state. The full scope of the metabolic reactions behind tumour progression is still a developing work, and the therapeutical advantages of using such knowledge remained to be broadened.

1.5.3.pH relevance for cancer metabolism

pH of cells and tissues is the result of cellular metabolic activities, ion transport and buffering systems. Regarding tumours microenvironment, it has been shown throughout the decades that intracellular pH (pHi) is slightly alkaline, while extracellular pH (pHe) is acidic. As already stated, tumour acidosis is mainly attributed to the Warburg effect, since this phenomenon has been observed in about 70% cancers. The excess of lactate from the high glycolytic rates together with limited buffering systems in the extracellular

microenvironment leads to the decrease of the pHe. However, simultaneously, cells are capable to maintain a steady normal/alkaline pHi, due to ion transport systems such as MCT (monocarboxylate transporters) family of lactate transporters, and protons transport systems (Na^+/H^+ exchange (NHE) and vacuolar H^+ ATPases (31).

Low pHe values are the result of cancer cells aberrant metabolism. Thus, tumour acidosis is directly linked to tumours metabolism, which allows researchers to make use of pHe as a marker to analyse the performance of anticancer agents, which act on cells metabolism.

Differences in pHe are caused by interference with several metabolic pathways. Fatty acid synthase is upregulated in cancer cells (29). It corresponds to the pathway used by cells to produce fat acids. By interfering with this pathway, ATP formation would decrease, as a result of a lower energy demand and pHe would consequently decrease. For detached cells, fatty acid oxidation is an essential sequence of reactions leading to energy formation and cells survival when the glucose uptake is impaired. Inhibiting PI3K/AKT/mTOR signalling pathway would also decrease lactate production and, therefore, reduce pHe (29). These changes in pH values in cancer microenvironments can be detected *in vivo* through imaging techniques such as magnetic resonance imaging (MRI) or positron emission topography (PET) (31).

1.5.4. Optical methods for pH measuring

We can go back in time regarding optical pH sensing as late as the 1970s, when pH stripes for pH became available commercially. In these, azo dyes are trapped through covalent bonds on a cellulose matrix (24).

Optical pH sensing is a broad field of different methods that can be used in the most diverse applications. The most common optical systems are absorptiometry, reflectometry, luminescence, fluorescence, refractive index, Infrared and Raman spectroscopy, surface plasmon resonance, and even photonic crystals (24). Phenol red is the most well-known pH sensing system used for cell culture monitoring. pH changes leading to structural modification in phenol red can be analysed using absorption methods (24). Luminescence intensity, more specific fluorescence intensity can be quantified making use of phenomena, like FRET (Förster Resonance Energy Transfer) and quenching of fluorescence. In FRET, for example, two different fluorophores are used, where the emission band of one must overlap with the absorption band of the other (24). The first one is excited, and the energy is transferred to the second one, which emits it, in the form of radiation. FRET is often applied in pH sensing, producing changes in

fluorescence caused by pH variations, being fluorescein/rhodamine B, a common fluorophores pair used for this purpose (24).

YinhuiLi et al. proposed a new set of fluorescence probes for NIR (near-infrared) fluorescence imaging for *in vivo* pH monitoring. The synthesized probes consisted of an hemicyanine skeleton with different substituent groups. These fluorescence probes have two emission bands, allowing the ratiometric fluorescence intensity quantification. The compound with benzothiazole as the substituent proved to be, overall, the most efficient chemical for the presented task, with a shift in the emission spectrum, from 672 nm to 748, of 76 nm and pKa approximately of 7, attributed by the researchers to its high intramolecular charge transfer (ICT). The intensity of fluorescence in each of these wavelengths is pH dependent, increasing or decreasing according to more acidic or basic solutions. Thus, the probe was calibrated in buffer solutions in the range of 6.5 to 7.8 pH values and also calibrated in the intracellular environment. It was also tested for the influence of different oxidative stress agents in the obtained pH value and, finally, its performance was determined in *in vivo* assays for acute inflammatory responses in mice (32).

In another example non-related with pH measurement, Weitai Wu et al. made used of materials pH-dependency to develop a hybrid nanogel chitosan based containing CdSe quantum dots used for drug delivery in tumours sites. These nanogels are formed by chitosan chains, crosslinked PMMA (Poly (methyl methacrylate)) and CdSe quantum dots. From three of the produced nanogels, the one covalently crosslinked presented the most desirable characteristics. These nanogels are pH responsive, in which the $-COO^-$ (PMMA chains) and $-NH_2$ (Chitosan chains) get protonated or deprotonated according to the pH of the microenvironment, while the CdSe QDs are used for biosensing and imaging. The protonation/deprotonation of these groups result in size changing of nanogels, due to changes in hydrogens bonds and coulombic interactions. For pH between 5 and 6.5, the nanogels size was reduced, due to, mainly, the $-COO^-$ and NH_3^+ attraction. For pH smaller than 5, the nanogels size increased, as a consequence to the full protonation of $-COO^-$ groups and enhancement of hydrogen bonds between PMMA and chitosan. Drug delivery and its release via these synthesized nanogels was study in mouse melanoma cells B16F10 using the anticancer drug temozolomide (TMZ). When pH increased the -COOH groups were deprotonated which broke the bounds formed between PMMA and TMZ and the nanogels swelled, resulting in the increase of TMZ mobility and its diffusion. Therefore, the researchers proved that drug release can be pH regulated through pH range in tumours sites (33).

1.5.5. Electrochemical methods for pH measuring

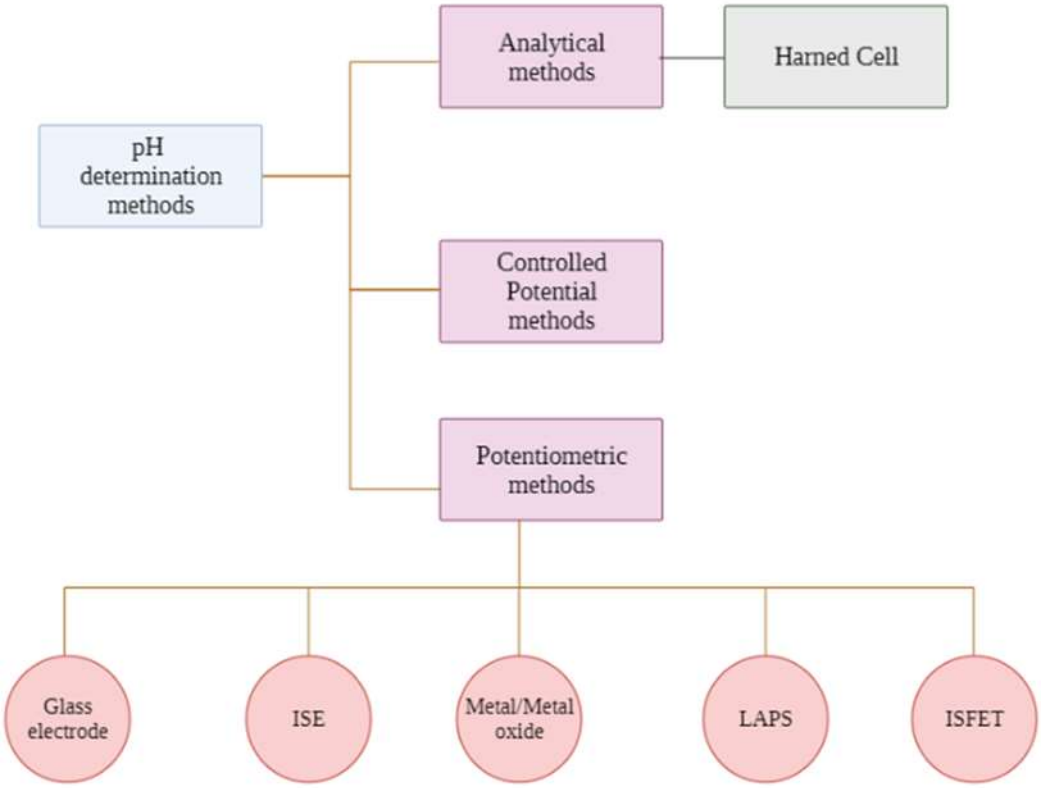

Figure 4. Different quantitative electrochemical methods used to determine pH (created in biorender)

According with the IUPAC (International Union of Pure and Applied Chemistry), electrochemical methods for pH measuring can be primary and secondary methods. Harned cell is the only method that allows to obtain an absolute pH value (34). The Harned cell is formed by platinum hydrogen gas electrode, and a silver/silver chloride reference electrode with no liquid junction. Firstly used for determination of activity coefficients, soon this cell started to be used to accurately measure pH (34).

1.5.5.1. Potentiometric pH sensors

A large majority of pH sensors have working principle based on potentiometry. This method requires a reference electrode and a sensing electrode. The set of electrodes is immersed in a solution of unknown pH and in chemical equilibrium, the potential difference is measured. The pH is linearly correlated with the measured potential according to the Nernst Equation (Equation 4) (35). The reference electrode has a known electrode potential, which does not vary with the samples while the sensing electrode develops

a potential, which depends on the activity of the analyte. The third component of a potentiometric cell would be a salt bridge that prevents the components of the analyte solution from mixing with those of the reference electrode. This can be implemented in different ways, not always needing the presence of a salt bridge (36).

$$E_{cell} = E_f^{\circ}(X/Y) - \frac{RT}{nF}\ln\left(\frac{[Y]}{[X][H^+]^m}\right) \Leftrightarrow$$

$$E_{cell} = E_f^{\circ}(X/Y) - \frac{RT}{nF}\ln([H^+]^m) - \frac{RT}{nF}\ln\left(\frac{[Y]}{[X]}\right) \Leftrightarrow$$

$$E_{cell} = E_f^{\circ}(X/Y) - 2.303\frac{mRT}{nF}pH - \frac{RT}{nF}\ln\left(\frac{[Y]}{[X]}\right) \Leftrightarrow$$

$$E_{cell} = E_f^{\circ}(X/Y) - 2.303\frac{mRT}{nF}pH \qquad \text{Equation (4)}$$

1.5.5.1.1. Glass electrode

The pH glass electrode is the most conventional pH sensor. It is formed by a glass bulk, which separates an inner reference electrolyte (with known pH) from the outer measurement medium (with unknown pH) (37). The glass contains SiO_2 and LiO_2. The protons present in each solution are attracted to the negatively charged oxygen in these materials, creating a soaking layer in each side of the glass membrane. These two layers have a defined electrochemical potential according to the pH value of their surrounding solution, which can be measured, due to the conductivity generated by positive cations present in the glass lattice. However, with time, the sensitivity of the glass electrode suffers a decrease due to the dissociation of groups in the glass surface, leading to slopes smaller than the Nernstian slope (≈59 mV/pH, 25°C) (37).

1.5.5.1.2. Ion Sensitive Field Effect Transistor (ISFET)

A field-effect transistor (FET) is typically formed by three terminals; the source, drain, and gate. There are two main types of FET: Junction Field Effect Transistor (JFET) and Insulated Gate Field Effect Transistor (IGFET). Both types distinguish themselves by the presence of an insulator between the gate and p or n semiconductor substrates. Conventionally, electronic circuits contain MOSFET (Metal Oxide

Semiconductor Field-Effect Transistor), which are semiconductor transistors that have a metal oxide, frequently silicon dioxide, as an insulator, preventing current flow from the channel and the gate (38).

For a structure where the source and drain are n-type and the substrate is p-type: if the voltage of the gate is positive, the positive charges (free holes) are pushed off from the region of the semiconductor placed under the gate. As the positive charges descend into the substrate a depletion region is formed. The depletion region becomes filled with negative charges. Meanwhile, the positive gate potential attracts the electrons present in the substrate towards the region close to the gate. The increased number of electrons induce the formation of a n-channel under the gate (inversion layer), which establishes a connection between source and drain. By applying a voltage between source and gate, a current begins to flow through the newly formed channel. The voltage of gate controls the current between source and drain (39).

These structures can be applied to sensing, including pH sensing. The sensing mechanism is activated by the binding of charged molecules or changings in the charges close to the gate.

Ion Sensitive Field Effect Transistor (ISFET) is theoretically like the MOSFET only varying in structure. In a ISFET the metal gate of a MOSFET is substituted by an ion-selective membrane, electrolyte and a reference electrode (Figure 6A) (39).

Although this type of biosensors can be miniaturized, facilitating their integration in microfluidic platforms previously described, and have a low cost and fast responses times, these sensors have a low sensitivity and can be affected by light, producing drift and hysteresis effects (35).

1.5.5.1.3. ISE – Ion Selective Electrodes

As all potentiometric sensors, an ISE is formed by a reference electrode and a sensing electrode. The conventional structure of the sensing electrode consists of a conductive electrical material, an inner filling solution and an ion selective membrane (40). In this type of potentiometric sensors, the ion-to-electron transduction is achieved by the reversible redox reaction that occur inside the inner solution. However, due to the difficulty of miniaturization, changes in pressure and temperature of the inner solution and potential drift, another structure of ISE has been proposed: an all-solid-state ISE, in which the inner filling solution between the sensing membrane and the electron conducting substrate is replaced by a solid contact (Figure 6B) (40). Depending on solid contact used, the transduction mechanism can consist in redox reactions or a double layer capacitance. The sum of potential differences of all the interfacial

potentials within the cell represent the final potential value used to calculate the concentration of the analyte (40).

1.5.5.1.4. LAPS – Light Addressable Potentiometric Sensor

Light addressable potentiometric sensor is a technique that, similarly to ISFETS, makes use of properties of semiconductors to perform potentiometric measurements (36). LAPS detect variations of the capacitance of the depletion layer. A typical structure of a LAPS device consists of a silicon layer, of n or p type, followed by a silicon dioxide layer and a silicon oxynitride coating (Figure 6C) (36). As the result of a bias voltage applied between a reference electrode and the silicon substrate, this last one becomes depleted of its charges. The incidence of radiation causes absorption of photons by the semiconductor layer and generation of photocarriers (electrons and holes) that reach the depletion region. These charges are separated due to the electric field inside the depletion layer which is transduced in a transient current. In the absence of light, electrons and holes merge and the resulting transient current has the opposite direction (41). The surface potential can be then calculated through the photocurrent generated, and the analyte concentration determined according to the Nernst equation. LAPS has been then used as a pH sensor since the oxynitride layer is pH sensitive (36)(41).

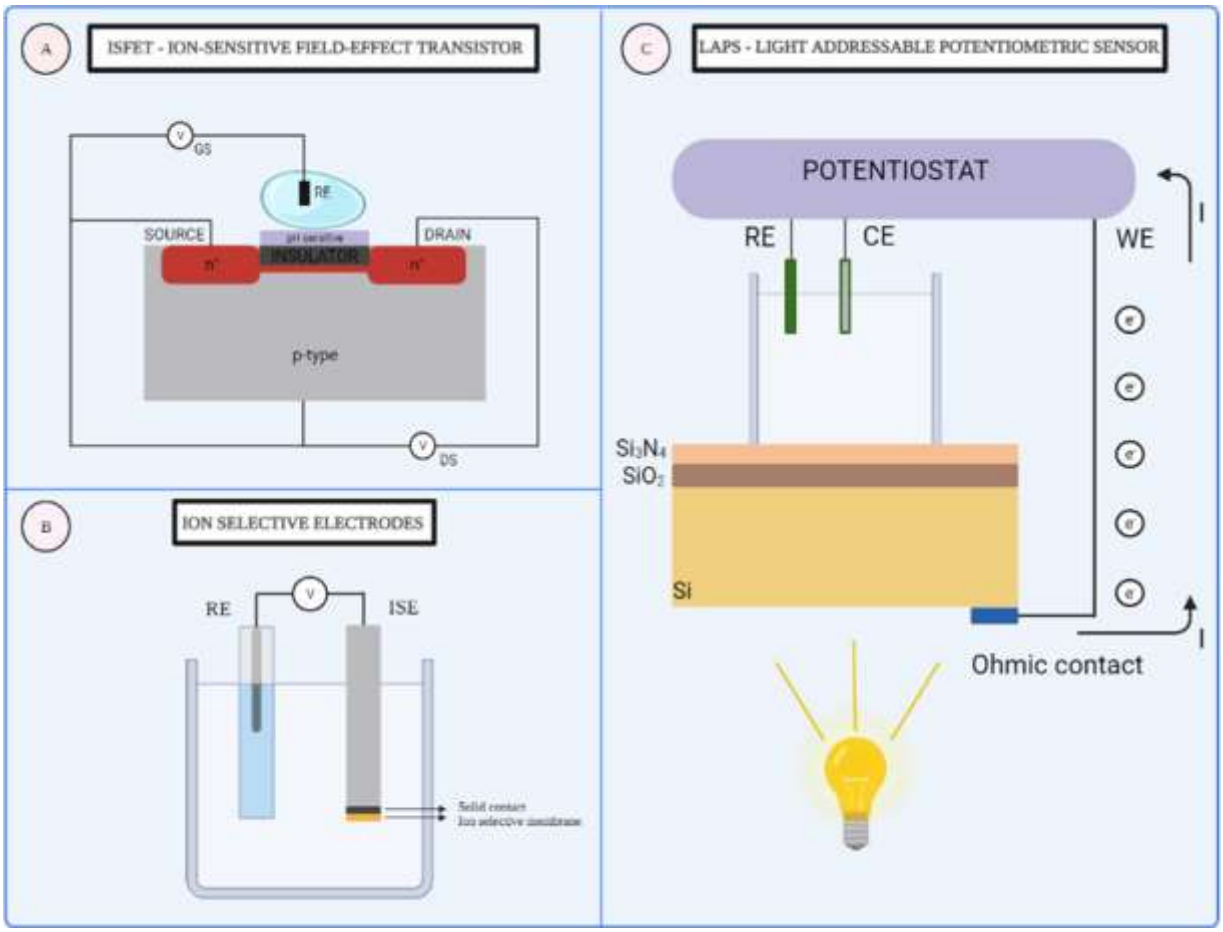

Figure 5. Schematic representation of ISFET (A), ISE (B) and LAPS (C) (created In biorender and adapted from Libu Manjakkal et al (35), Jinbo Hu et al (40), and Tatsuo Yoshinobu et al (41))

1.5.5.1.5. Metal oxides

Metallic materials are often used to build sensing electrodes as it was observed in the previous examples given. They can be used for metal oxide deposition, where only the metal oxide is involved in the pH dependent electrode reaction and serving only as the electronic conductor. Several metal oxides are used for pH sensing, such as Tantalum oxide (Ta_2O_5), Titanium oxide (TiO_2), Zinc oxide (ZnO), Lead oxide (PbO_2) and Ruthenium oxide (RuO_2) and Iridium oxide (IrO_2), being these last two considered the most promising ones in the field (35).

1.5.5.1.5.1. Iridium oxide-based electrodes as pH sensing system

Carbonate melt oxidation of iridium wire, reactive sputtering methods, thermal decomposition, and sol-gel deposition lead to anhydrous IrOx films, which results in a near-Nernstian response with a sensitivity

of approximately 59 mV/pH, where one electron is transferred for each proton in the redox reaction (Reaction 1). On the other hand, a super-Nernstian response, with a sensitivity higher than 59 mV/pH is associated with hydrated IrOx films, produced by electrochemical methods (Reaction 2). As a result of these hydrated IrOx layers, the number of transferred electrons is smaller than the number of hydrogen ions (42).

Reaction (1)

$$2IrO_2 + 2H^+ + 2e^- \rightleftharpoons Ir_2O_3 + 2H_2O$$

$$2[IrO_2(OH)_2.2H_2O]^{-2} + 3H^+ + 2e^- \rightleftharpoons [Ir_2O_3(OH)_3.3H_2O]^{-3} + 3H_2O$$ Reaction (2)

In the formed porous and hydrated AIROFs (Anodically electrodepositing iridium oxide films), there is an excess of hydroxyl groups adsorbed on the metal oxide film surface, depending on the oxidation state of the iridium oxide groups (43). Ir (IV) oxide are Lewis acidic centers, which justifies the adsorption of OH^- groups, unlike the Ir (III) oxides, which are less acidic than the oxidized form. It has been hypothesized that the presence of these hydroxyl groups increases the proton exchange, and consequently, the sensors sensitivity (44). Besides, the existence of both oxidation states is probably the reason why the sensitivities, using this method of deposition, present variability (43).

Iridium oxide sensors have been fabricated and applied for several applications, always with the purpose of real time monitoring of pH. In 2017, Bo Zhou et al. presented a miniaturized multiparameter sensing platform to evaluate water quality, through the parameters: pH, temperature, and conductivity. The silicon chip was made through conventional MEMS techniques, where the pH and reference electrode were further integrated. The pH sensor was made by electrodeposition of the iridium oxide deposition solution prepared according with Yamanak et al method, using Cyclic Voltammetry. Additionally, they produced an Ag/AgCl reference electrode coated in a platinum wire, with a solid inner electrolyte made of KCl saturated agar gel, avoiding the liquid junction issues. Calibrations were done in pH standard solutions in a range of 2.22 to 11.81. The researchers obtained a -67.60 mV/pH sensitivity, with a maximum difference between tests of 16 mV, and response times smaller than 7s (45).

This type of sensors has also been tested in cell culture environments, for the purpose of studying extracellular acidification. Shu Rui Ng reported an AEIROF to monitor local pH changes of PAECs (porcine

aortic endothelial cells). The MEA (microelectrode array) chip was composed of silicon nitride, where the pH electrode was implemented. After anodic electrodeposition of IrOx films on top of gold microelectrodes, the chip was coated with poly(ethyleneimine) (PEI) to give mechanical stability to its sensors. After PEI coating, fibronectin was chosen as the ECM component to provide a matrix for cells attachment to the chip. For cellular experiments, the chip was inserted inside a glass chamber with cell culture medium, where the Ag/AgCl reference electrode was posteriorly added for potentiometric measurements. These pH sensors presented a sensitivity of (0.066 ± 0.03) V/pH in chloride-free phosphate buffers for a range between 4 and 7.7. Response times were also determined for different pH values, resulting in a maximum of 190.2s for pH 7.7 and a minimum of 0.3s for pH 4. The MEA chip was tested for local pH changes measurements in the presence of cells and in a control condition without cells. The investigators concluded that the chip responded to the addition of factors such as thrombin and the MAPK inhibitor, PD98059. As a result of fibronectin dissolutions, thrombin caused a pH decrease, and consequently, cells detachment. In contrast, and as expected, the addition of the inhibitor lead to a rise in pH. This work showed the construction of a pH sensor device which can successfully detect metabolic changes in cells through stimulus that induce local pH changes (46).

2. Project goals and strategies

This work was developed inside the context of the N2020 FROnTHERA project, in collaboration between INL and 3Bs. The objective consisted in develop and optimize a pH sensing system for the pH long term monitoring of pH in cell culture systems. Initially it was applied in a multiwell plate to be used, for example in anticancer drug assays. In the future it would be implemented in an organ-on-chip reactor, where breast cancer cells (MCF-7) would grow inside a gellan gum scaffold and their microenvironment pH would be monitored in real time, over long periods. The sensors would be implemented inside the hydrogel, at different heights to measure the pH microenviroment, and its possible changes at different positions inside the matrix. The main tasks for this project are:

- Design and development of a cell culture model system for cell metabolite sensing
- Development and optimization of a pH sensing system
- Integration of the electrochemical system in a 2D cell culture model (multiwell plate)
- Monitor and optimize the growth of cells in device using optical microscopy
- Integration of the electrochemical system inside the bioreactor for monitoring pH changes and its impact on 3D tissue culture.
- Monitor and optimize the growth of cells in the device using optical microscopy

3. Materials and Methods

3.1. Materials and reagents

Double tooth cutter with fishtail milling tools (3 mm, 2 mm), were purchased from the company vhf. Dow Corning Sylgard® 184 polydimethylsiloxane (PDMS) was purchased from Ellsworth Adhesives Ibérica (Madrid, Spain). Iridium chloride hydrate ($IrCl_4.H_2O$, 99.95%,), hydrogen peroxide (H_2O_2, 30%, aq), oxalic acid dihydrate ($(COOH)_2.2H_2O$), anhydrous potassium carbonate (K_2CO_3), titanium (0.25 mm of diameter, 99.7%), platinum (0.2 mm of diameter), silver (0.5 mm of diameter, 99.99%) wires, ethanol, sulphuric acid (HCl), potassium chloride (KCl), sodium hydroxide (NaOH), calcium chloride ($CaCl_2$) phosphate buffered saline, Nafion™ perfluorinated resin solution (20 wt. %), sodium alginate, Dulbecco's Modified Eagle's Medium (DMEM) and human recombinant insulin were purchased from Sigma-Aldrich (St. Louis, MO, USA). trypsin-EDTA (0.25% trypsin; 0.1% EDTA), penicillin/streptomycin 100x, Fetal Bovine Serum (FBS) were purchased from Merck Millipore (Burlington, MA, USA).

3.2. Fabrication of the bioreactor

3.2.1. Design of the cancer-on-a-chip system

The design was made using AutoCAD and ArtCAM softwares. It consists of two channels: upper and lower, both connected to a chamber located in the centre of the device. The upper channel leading to the inlet and the lower channel leading to the outlet. On top of the two PDMS layers resides a detachable piece with an opening standing above the chamber to allow the electrodes to reach the inside of it.

(a)

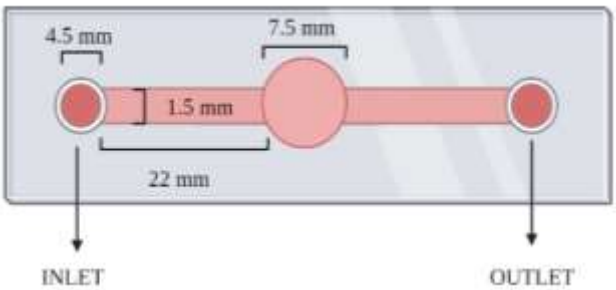

(b)

(c)

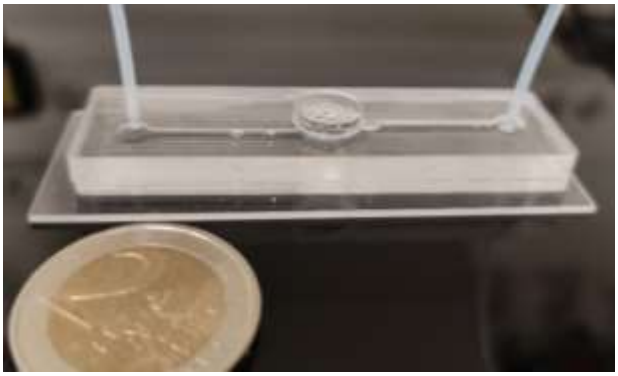

Figure 6. Schematic representation of the organ-on-a-chip system from the top view (a) the side view (b), real depiction of the bioreactor (c) (created in biorender)

3.2.2. Fabrication of the cancer-on-a-chip system

A FlexiCAM viper CNC machine (FlexiCAM Viper CNC, FlexiCAM GmbH, Eibelstadt, Germany), was used to create the moulds in acrylic plastic (PMMA) for the construction of the different pieces of the device, using the design elaborated in the mentioned softwares. The moulds were filled with poly(dimethylsiloxane) (Sylgard 184 PDMS pre-polymer and curing agent), in a 1/10 ratio (wt/wt), to create the two parts of the device: two layers fixed together to create the channel system along with the chamber that contains the gellan gum-based hydrogel. The PDMS was baked for 2h at 65°C. The lid, meant to cover the chamber, was fabricated using the Laser Engraving Cutting system (Widlaser LS1390 Plus, Widinnovations) with PMMA as material. These PDMS pieces were bonded through plasma oxygen treatment for 30 seconds, using a Plasma Cleaner instrument ((Harrick Plasma Cleaner). On the base, a glass slide was used to support the device and allow, simultaneously, the microscopic visualization of cells inside the hydrogel.

3.3. Development of the pH sensing system

3.3.1. Preparation of the solution for Iridium Oxide deposition

The iridium oxide deposition solution was prepared following the procedure described by Yamanaka et al. (47). First, 15 mg of Iridium chloride hydrate ($IrCl_4.H_2O$, 99.95%) was dissolved in 10 mL of distilled water, by magnetically stirring the solution for 30 min. Thereafter, 0.1 mL of aqueous hydrogen peroxide (H_2O_2 (aq), 30%) was added, and the solution was stirred for another 10 min. This was followed by adding 50 mg of oxalic acid dihydrate ($(COOH)_2.2H_2O$) and 10 minutes of stirring. The pH of the solution was adjusted by slowly adding small portions of anhydrous potassium carbonate (K_2CO_3), into the solution, until a pH

of 10.5 was reached. The latest prepared solution presented a yellowish coloration. As stated in the literature, the solution was covered and left to stabilize for 2 days, at room temperature. During this period, the colour of the solution changed from yellow to blue and finally, a vivid violet. After stabilization, the fresh solution was kept in the dark at 4°C. This solution should only be used for a 2-month period. As the solution ages, the stabilization times obtained increase (42).

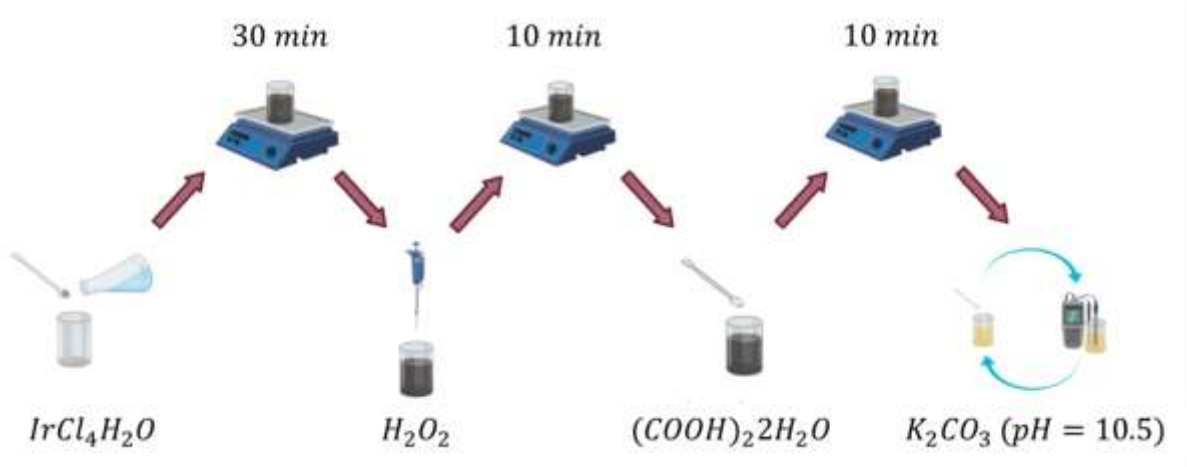

Figure 7. Schematic representation of the preparation of the deposition solution (created in biorender)

3.3.2. Wire Sensing Electrodes preparation

Both titanium and platinum electrodes, with diameters of 0.25 mm and 0.2 mm, respectively, were cut into 5 cm pieces. The electrodes active area (9.42 mm^2) was covered with regular tape, while the uncovered part of electrode was coated with nail polish, except for the tip of the electrodes, which is responsible for establishing the electrical contact with the external electronics.

3.3.3. Anodic electrodeposition of IrOx coating

The electrodeposition of metal oxides involves the oxidation of metal ions present in solution followed by its precipitation and the formation of a film. Electrodeposition may be anodic or cathodic. In cathodic electrodeposition, there is a reduction, occurring on the cathode, while in anodic electrodeposition, there is an oxidation happening in the anode.

Iridium oxide was deposit on the surfaces of titanium or platinum wires by anodic electrodeposition. Platinum wire was used as cathode. The first step consisted of cleaning the surface of the electrodes through successive oxidations and reductions by performing a Cyclic Voltammetry (CV) in the range -0.23 V to +1.1 V at 100 mV/s rate for 20 cycles, in a H_2SO_4 solution (0.5 M) (9.42 mm^2). After the cleansing, a current density of 1 mA/cm^2 (0.1 mA for a 9.42 mm^2 area of wire) was applied for 20 minutes, while

the electrodes were dipped in the prepared deposition solution (47). Once the deposition was completed, new pH sensors were rinsed with distilled water and dried under a stream of nitrogen. Both the CV and the anodic electrodeposition were done using Keithley Sourcemeter 2400. The sensors presented a blue-black coloration as expected according with Yamanaka et al protocol. The freshly made sensors remained dipped in PBS buffer (pH=7) for at least two days, before usage, for stabilization purposes (48).

3.3.4. Nafion coating of IrOx based sensors

After the iridium oxide electrodeposition, the sensors were dipped in Nafion solution (2% or 5%) and baked in the oven at 65°C (42)(49). This procedure was always repeated twice for each fabricated sensor, according with the protocol in Sayed A. M. Marzouk et al (49).

3.3.5. Preparation of Reference electrode

Initially, a pseudo-reference electrode was used. This electrode was made of silver wire, with a diameter of 0.2 mm, with a silver chloride coating. First, the silver wire was polished. Thereafter, the silver chloride layer was deposited by applying 2.355 mA of current for 1 min, in a 0.1 M solution of HCl (current density of 10 mA/mm^2, in 9.42 mm^2 of area), being the silver wire the anode and the platinum the cathode. After the coating, the electrodes were rinsed with distilled water.

The reference electrode that substituted the pseudo-reference, was made using a micropipette tip and an alginate gel junction. The first step was sealing the end of the tip with cotton, followed by the insertion of a 2% sodium alginate solution inside the tip, and through the cotton. After the sodium alginate solution covers the entire extremity of the tip, a 3% calcium chloride ($CaCl_2$) solution was added to the top and bottom of the cotton structure embedded in sodium alginate, to crosslink the alginate. After a 5 to 10 minutes period for the crosslinking, the tip was filled with a 3M potassium chloride solution. In the last step, the Ag/AgCl electrode was dipped in the KCl solution of the tip, and the top was sealed with parafilm.

3.4. Recording system for potentiometric signals

3.4.1. Hardware

For collecting data, it was designed, and a built custom pH sensor interface composed of an electronic module and a data acquisition software. Conceptual schematic of the system is depicted on figure 9. Electronic module begins with an analog front-end based on a low input current precision operational amplifier (LMP7721, Texas Instruments) with only 3 fA input bias current. We chose this amplifier to reduce any current drawn through the electrodes, which could cause over time drifts and electrochemical

degradation. Through the feedback resistors R1 and R2 amplifier was designed to have voltage gain 2x. Output signal of the analog front-end was converted to digital code by analog-to-digital converter (ADC), where we used 16-bit 100-ksps chip with serial SPI interface (ADS8866, Texas Instruments). Signal was collected and integrated over 256 samples by a microcontroller unit (MCU, ESP32-WROOM-32, Espressif Systems) and transmitted via USB to a personal computer (PC). We used serial (UART) to USB converter chip FT230XS (FTDI Chip) to connect MCU and PC. Electronic module was also powered through PC and did not have separate power supply. Before usage we evaluated the system to determine calibration parameters, exact range, and noise. Potentials were calibrated against precision voltage source (Keithley Sourcemeter 2400)). Determined parameters were: i) potential range from - 300 to + 1000 mV, ii) sample rate 9 samples/s and iii) noise 265 µV.

For the 2D cell culture system an electronic interface was built for pH measurements in a multiwell plate. The electronic system is very similar to the one mentioned above from the previous interface. The PCB board was made to fit perfectly with the 6 multiwell plate. It contains in its structure pin-sockets for the connection of sensing and reference electrodes for the six sets. The PCB was then adjusted to an acrylic piece that served as a support. This structure represents the multiwell lid, placed above the wells, allowing for the attached electrodes to be dipped inside cell medium in each well (Figure 28). The lid is connected by a standard RS232 cable with DB9 connectors to an Arduino system, which function is to convert the analogue signals received from the lid into digital signals and transmit them to the computer, over a USB port. The interface range goes from -200 to 1200 mV, with a noise lesser than 2 mV.

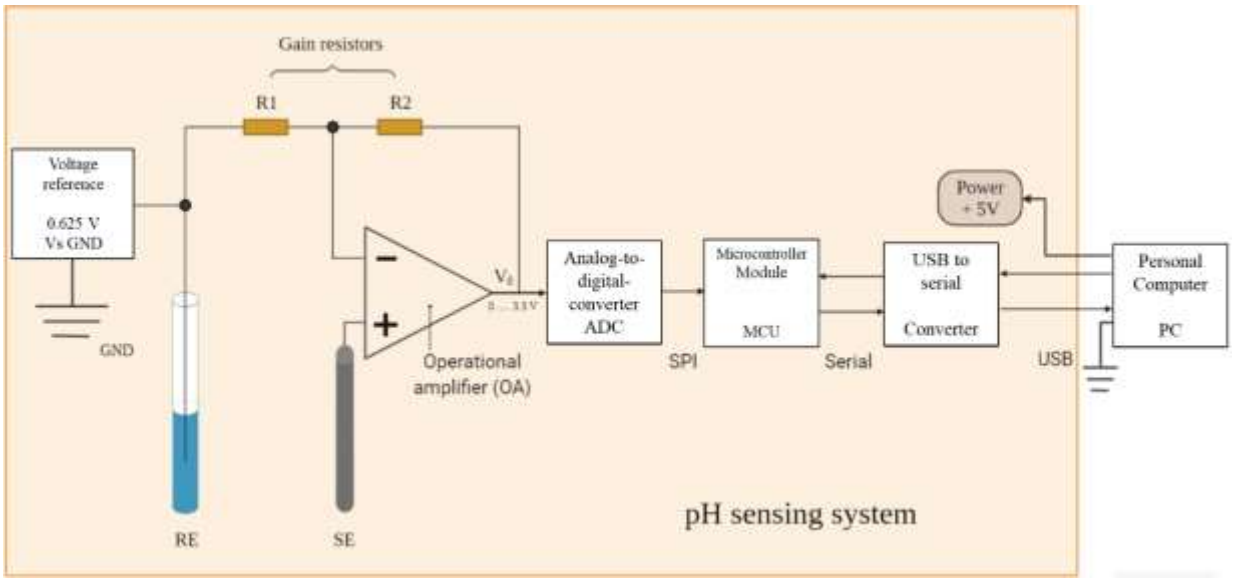

Figure 8. Schematic representation of the in-house-made electronic interfaces (created in biorender)

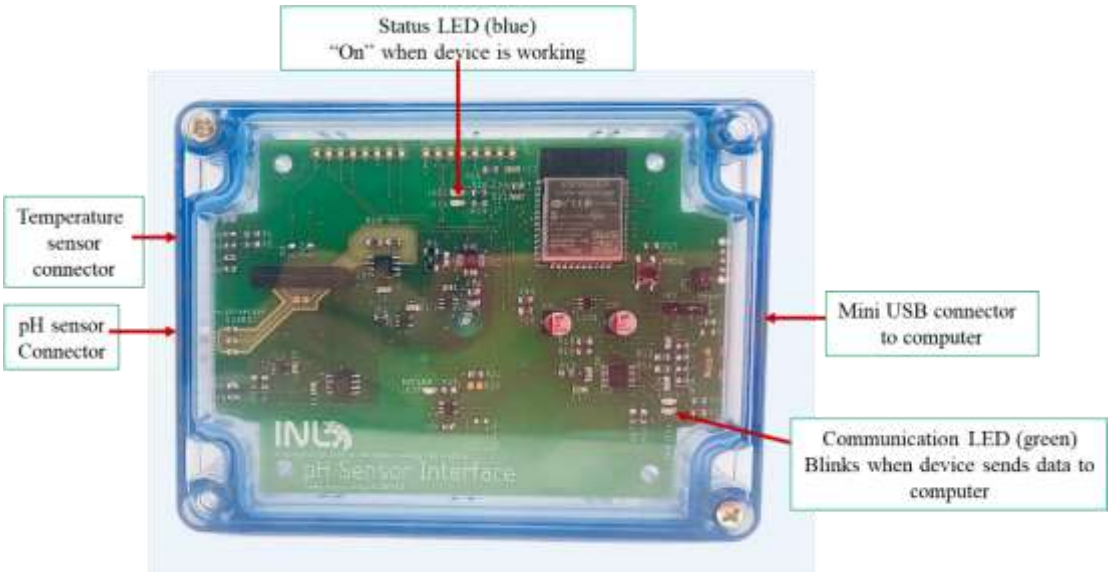

Figure 9. Schematic Representation of the in-house-made electronic interface

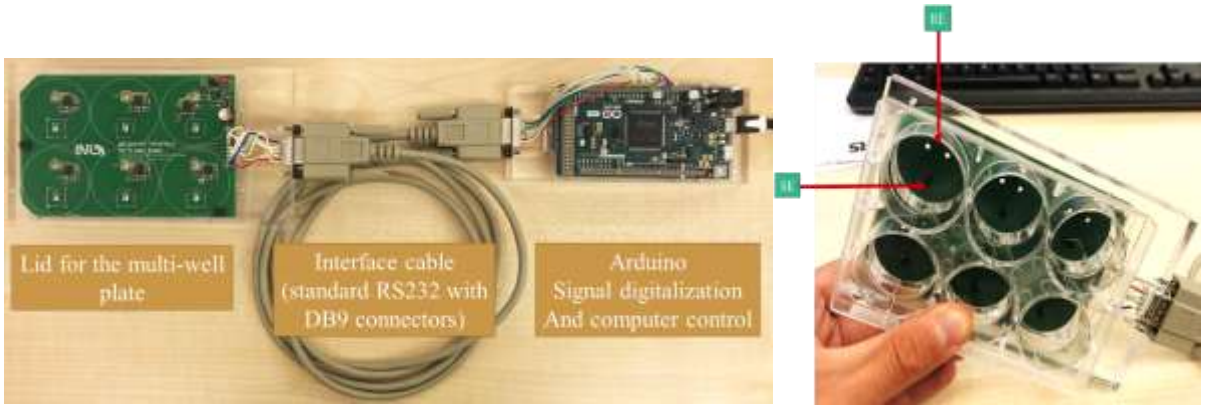

Figure 10. Schematic Representation of the in-house-made electronic interface for the 6 multiwell plate

3.4.2. Software

In order to view and collect data from the built interfaces an app was developed. For designing the data acquisition software, we used Visual Studio, .NET framework (Microsoft) and C sharp programming language. This software allowed to connect to the electronic module through serial (COM) port, receive data, adjust calibration parameters, and convert digital codes to mV values, visualise and save collected data (Figure 11).

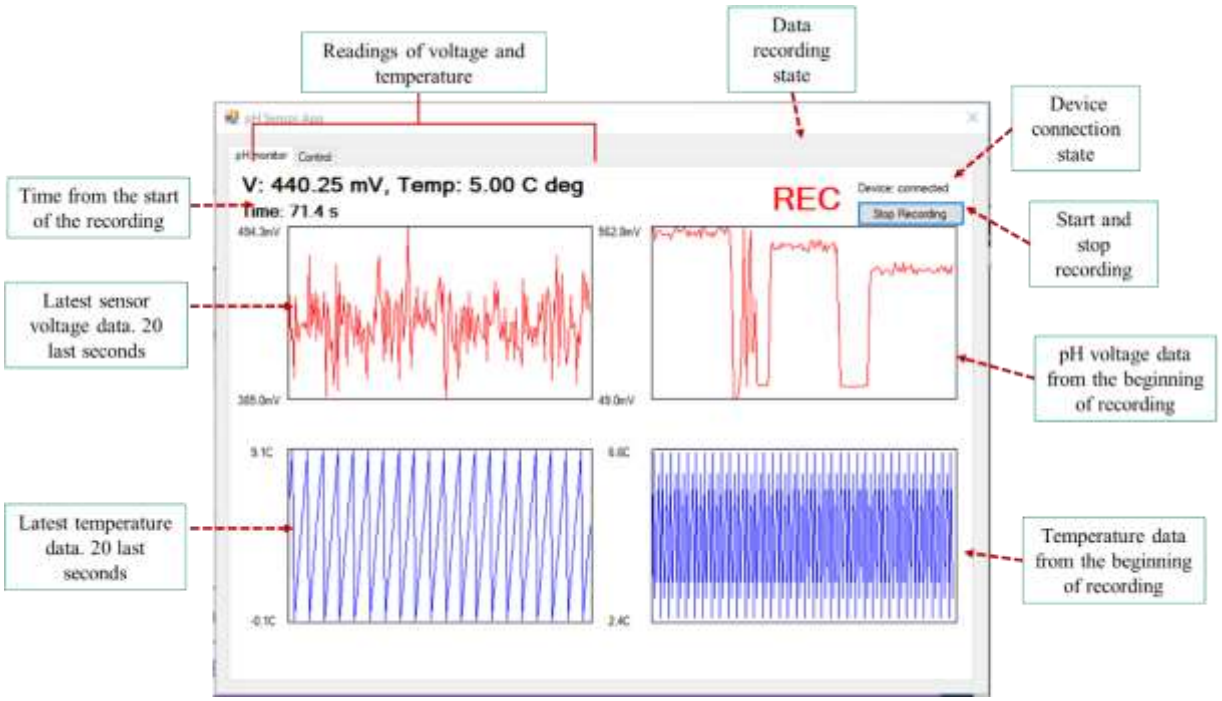

Figure 11. Schematic representation of the windows app developed for the electronic Interface

3.5. pH measurements

The pH sensors were first tested in phosphate-buffered saline (PBS) buffer solutions (10 mM) with pH values ranging from 6.4 to 7.5. For pH changing two reagents were used: hydrochloric acid (HCl) in two different concentrations, 0.1 M and 1 M as an acid, and sodium hydroxide (NaOH), with concentration of 1 M, as a base. The potential measurements of each pH buffer solution were made consecutively, with pH sensors being washed in Milli Q water in between.

Thereupon, the measurements were made in DMEM cell medium (Dulbecco's Modified Eagle's Medium), supplemented with 10% of Fetal Bovine Serum (FBS), 1% of Penicillin-Streptomycin, and 0.1% of human recombinant insulin. For starters, the pH measurements were done as for the buffer solutions. However, as it is further explained in section 4.2, the protocol had to be replaced by a titration-like approach. In initial experiments, the pH of solutions was measured using a standard pH probe (pH electrode InLab Expert Pro, Mettler Toledo) along with a pH meter (SevenCompact S220-Basic, Mettler Toledo) in a first instance, and only afterwards were the potential measurements made. By modifying the protocol, the pH solution of DMEM was changed by the continual addition of acid or base as the potential was being measure simultaneously with our pH probe. Thus, the pH was determined at the same time as the potential was being recorded. Once again, the covered range consisted of 6.4 to 7.5, approximately.

For the pH measurements done at 37°C, the procedure was the same as described previously, with the exception that the flask containing the DMEM solution was dipped in a water bath, heated by a hot plate, whose temperature was measured by a thermometer.

3.6. Cell culture monitoring in 6 multiwell plate

MCF-7 human breast cancer cell line was the one used for the multiwell experiments. The cells were sub-cultured in 25 cm^2 cell culture flasks. The medium used was DMEM (Dulbecco's Modified Eagle's Medium), supplemented with 10% of FBS, 1% of Penicillin-Streptomycin, and 0.1% of human recombinant insulin, and the cell line was kept at 37°C, in a humidified atmosphere with 5% of CO_2, inside the incubator.

For the cell seeding in the multiwells, cells were first detached from the flasks surface using trypsin-EDTA for 5 min. and transferred to the wells of the 6-multiwell plate, at a density of 31250 cells/cm^2. The multiwell plate was divided into two conditions: (1) three wells were seeded with cells and (2) three wells were used as control with DMEM and no cells, to serve as a baseline for each of the replicas.

The pH sensors and Ag/AgCl electrodes were, prior to the cell seeding, dipped into ethanol for disinfection, while the reference electrode with the alginate junction was fabricated in sterile conditions, with the reagents mentioned above having undergone heat treatment.

After the cell seeding, the sensing and reference electrodes were attached to the PCB lid, which was then, place on top of the multiwell plate. The sensors active area was, consequently, dipped in the cell medium of each well.

The potentials were recorded during a period of 3 days, with no interference being made, such as cell medium renewal.

3.6. Statistical analysis

The statistical analysis was performed in the MATLAB R2018b software. These functions consisted in previewing data recorded by the app created, processing that data and use the processed data for further analysis.

Three main functions were used recurrently, being those: (1) the one used to process the received data, (2) a linear fit function and (3) a calibration function that performed a linear fit to the data processed by the first function. In summary, a proper explanation of these functions is offered.

The first function task consisted in identifying the points where the signal was out of range, so those points could be excluded, and the stable signal area determined. The function made use of the noisy areas, which were produced by the change of solutions during the experiments, to define the area. In case such noisy spots didn't exist (titration experiments), then the stable area had to be chosen manually. The selective area could also be narrowed down by two input parameters inputs: the period before the first point is considered and the duration of the measurement. Once the data was selected, a statistical analysis of the data was applied, by calculating mean values of time and potential, standard deviation, and the average drift. The latter was given by the slope of a linear regression performed to the chosen data points.

For calculation of the linear regression equation, another complementary function was used, the linear function. This function was made using the least square methods, and it allows for the determination of slope and intercept of the linear regression, as well as their uncertainty as standard deviation values.

Moreover, another function was also use in the course of data analysis. This function purpose consists of determining the drift associated with the developed sensors, and it calculated the drift through determination of the linear regression slope.

At last, the curve fitting toolbox, available in MATLAB software, was used to build a polynomial function that adjusts to the data sets. The output parameters were the coefficients for the best polynomial fitting function with 95% of confidence level and the uncertainty associated with each coefficient.

4. Results and discussion

4.1. Testing of sensors in pH stable solutions

Initially, platinum was chosen as the electrically conductive material, in which the iridium oxide layer was deposited. However, due to the high cost of platinum, titanium wire was tested as an alternative, being more convenient for the mass production of electrodes.

These sensors were first tested in PBS buffer solutions (10 mM) with different pH values, in the approximately range of 6.4-7.5. The potential differences were measured using an in-house made electronic interface (Figure 9), and the respective potential values were determined after the signal stabilization. The measured values used to determine the average potential corresponding to each pH value are highlighted by the green region. The average value is marked as the red circle and the linear drift is represented by the magenta line (Figure S2). The different pH values are divided by noisy regions caused by the changing of solutions.

The calculated average of potentials for each pH value were further used for a linear regression analysis (using the least square methods) which establishes a linear correlation between pH values and potential values as described by the Nernst equation ($\Delta V = a^*pH + b$). The red line represents the best fit found for the data set, while the green line represents the confidence intervals at a confidence level of 95%, which means there is a 95% probability that any value obtain is inside this interval (Figure S2).

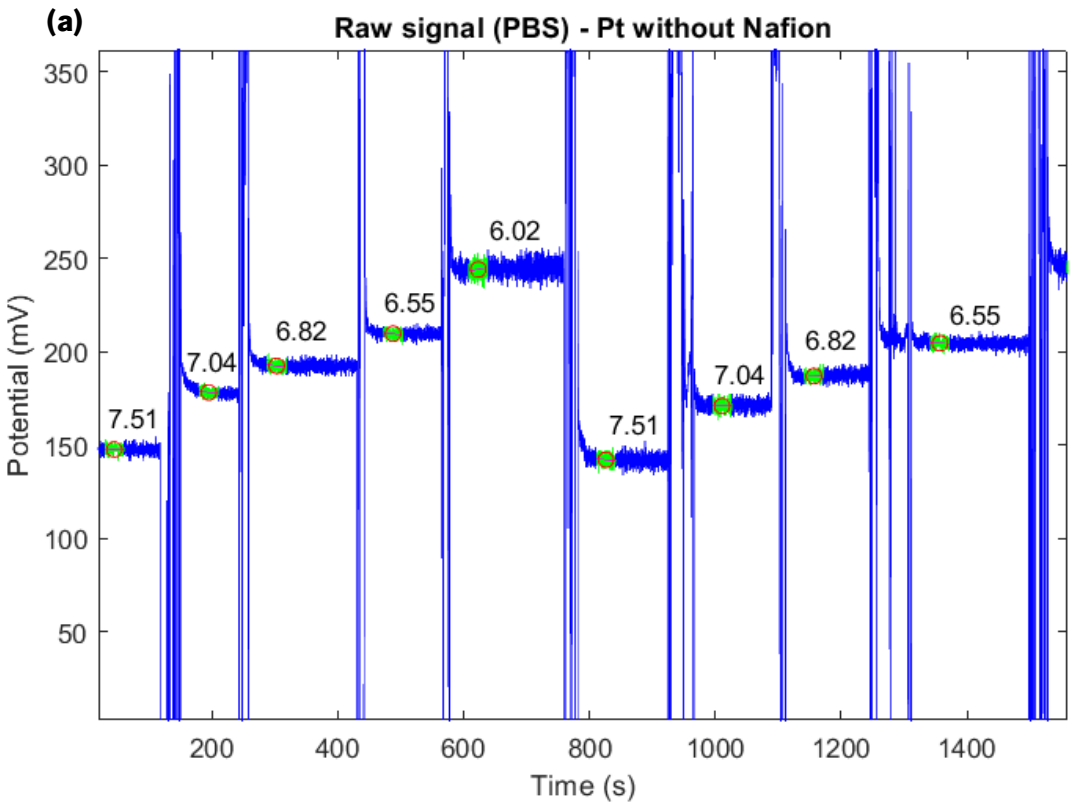

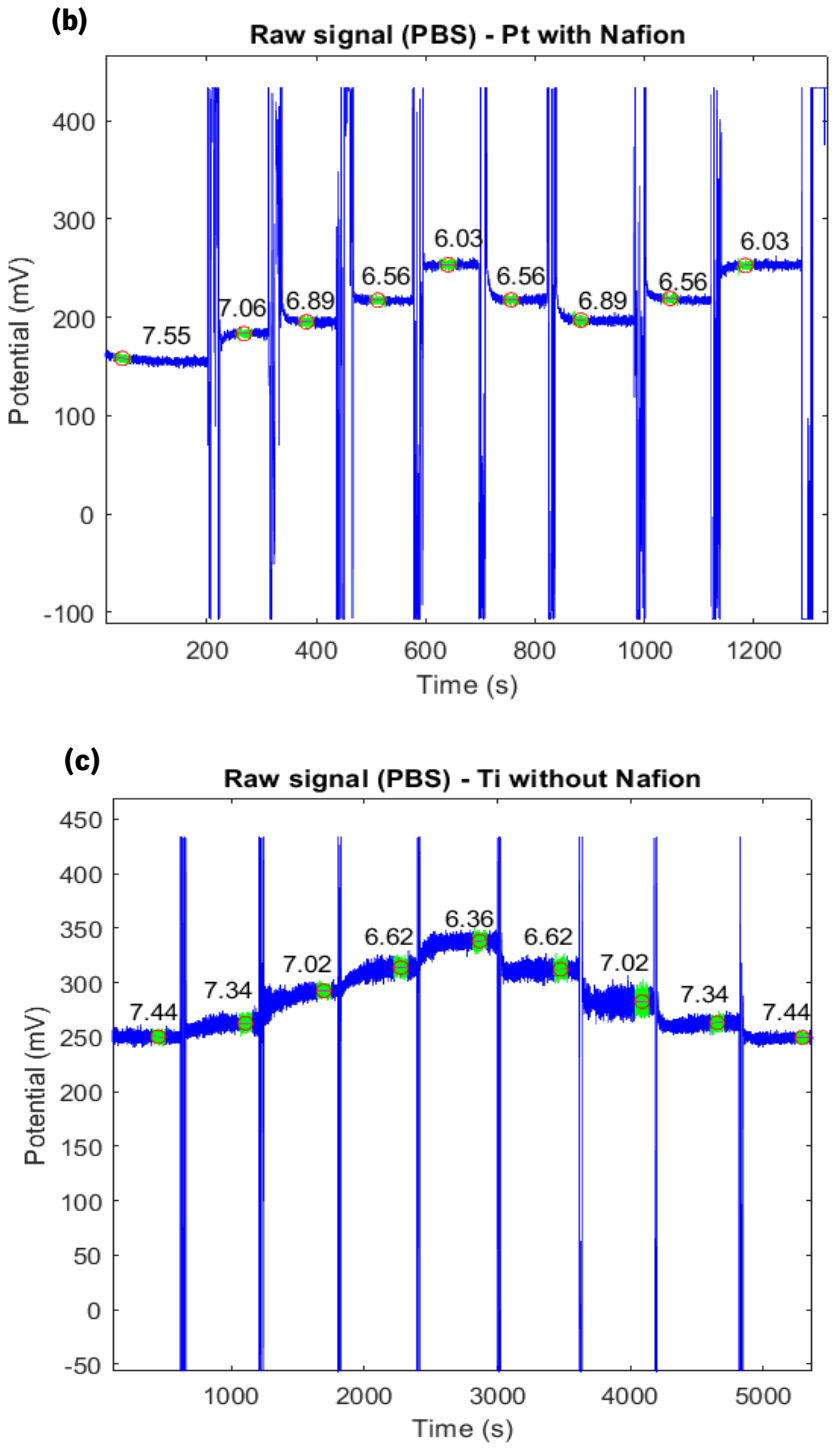

Figure 12. Raw signal of potential differences measured in PBS by the in-house-made electronic interface for platinum with IrOx coating (a), platinum with IrOx and Nafion coatings (b), and titanium with IrOx coating (c) sensors

Along with the slopes and intercepts of the best fitting equation, the uncertainties (standard deviation*t_value) associated with them were also calculated and represented in each graphic (Figure 13). These experiments were made using a pseudo reference electrode.

The sensors sensitivities, represented by potential variations per pH unit, are given by the slope of each fit. Sensitivities for all the tested sensors are superior to the Nernstian slope (≈-59 mV/pH), which is in agreement with what the literature shows according to the chosen method of deposition (49)(50). The errors associated with both slopes and intercepts were relatively small, an important detail for sensors accuracy. These results point out the good performance of such sensors for PBS solutions as samples. Besides that, it is crucial to underline the performance of the in-house-made electronic interface used to detect and convert the chemical signal into an electronic signal. For the same sensors (platinum with IrOx and Nafion coating), the sensor used with the in-house-made interface (Figure 13b) presented similar sensitivities compared with commercial pH meter used as the recording system (Figure 13d).

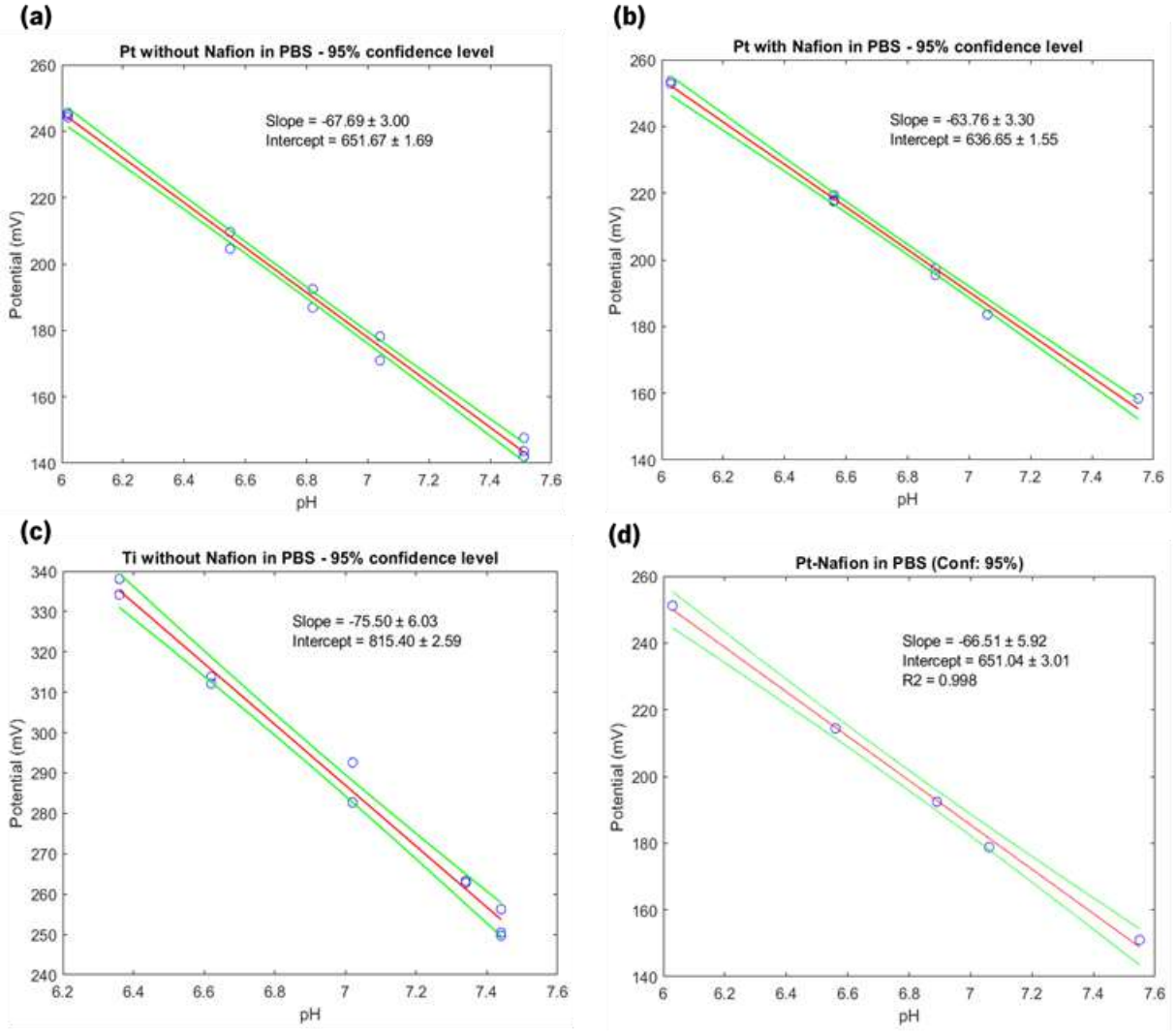

Figure 13. Calibrations (potential vs pH) done by the values measured in PBS by the house-made electronic interface for platinum with IrOx coated (a), platinum with IrOx and Nafion coated (b), titanium with IrOx coated (c) sensors and calibration with measurements done by a commercial pH meter (SevenCompact S220-Basic, Mettler Toledo) for platinum with IrOx and Nafion coated sensor (d)

The two types of sensors, with platinum and titanium as the conductive material, where the sensitive layer was deposited, responded to pH changes linearly, following a near Nernstian or super Nernstian behaviour, as described in the literature (50)(51)(52). Despite the suitability of both metals, titanium was the chosen material to use for the following experiments, due to mainly its low cost as mentioned above.

4.2. Testing of sensors in DMEM

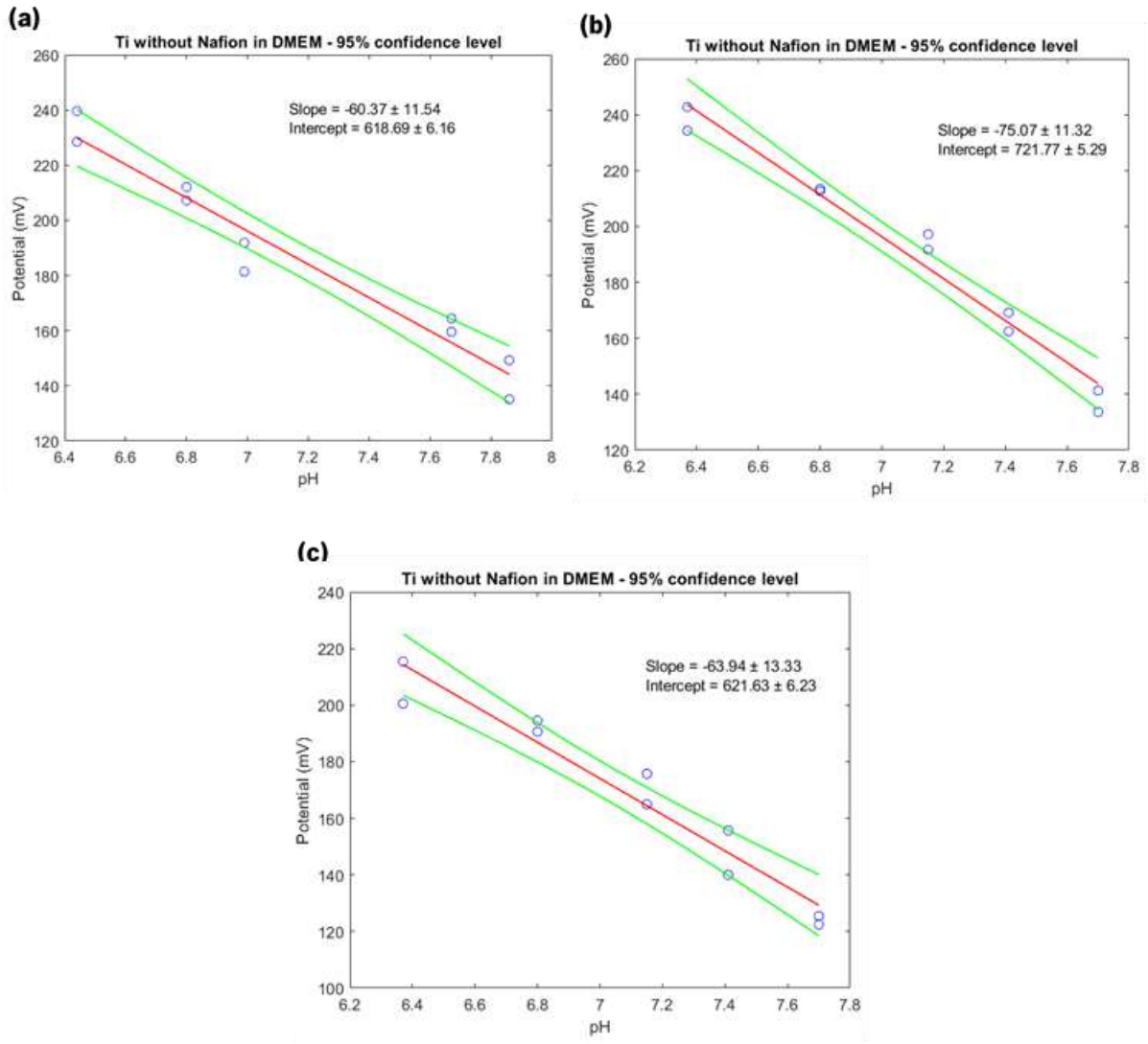

Figure 14. Calibrations (potential vs pH) determined in DMEM by the in-house-made electronic interface for titanium with IrOx coated sensors 1 (a), 2 (b) and 3 (c)

Despite the results demonstrating the good performance of the sensors, it was required to test this type of sensors in cell medium, given the purpose of applying them for cell culture monitoring. Cell culture medium is very complex in comparation to the buffer solutions previously used. It is composed by vast

amounts of different components required for cells, like sugars, aminoacids and vitamins, that may interact with the developed sensors, interfering with the signal and affecting the results.

Having this in mind, the same calibrations were made in DMEM medium with three replicas, to analyse the reproducibility of the sensors. These experiments were carried out with the samples in an ice bath, since they were kept in the fridge to prevent the fermentation of samples and temperature conditions between experiments must be the same for comparison purposes.

By observing the linear fittings presented in figure 14, it can be concluded that though the sensitivities are within the expected range as pointed out previously, the errors associated with both slopes and intercepts are twice as much as the errors obtained with the buffer solutions.

This difference compared to the results obtained in previous experiments with solutions with stable pH led to conclude that the increase in the error could be due to the difficulty of maintaining the pH stable in DMEM solutions. Such conclusion was reached by analysing the continuous change of pH of a DMEM solution, under constant magnetic stirring, without any addition of acid or base. By plotting the pH values against the potential values measured a fitting with a Nernstian slope was obtained (Figure 15b). This instability is caused by the differences in CO_2 concentration inside the incubator and at normal atmospheric conditions. Simple DMEM medium has sodium bicarbonate ($NaHCO_3$) as a buffering system to keep cell medium pH stable. Inside an incubator the CO_2 concentration is typically around 5%. The CO_2 dissolved in the cell medium reacts with water molecules and forms carbonic acid (H_2CO_3), inducing medium acidification. However, outside the incubator CO_2 concentration is lower, leading to the evaporation of the dissolved CO_2 in the medium, followed by consumption of carbonic acid and an increase in pH values. Stirring accelerates the release of CO_2 and a more rapid pH change.

$$CO_2 + H_2O \rightleftharpoons H_2CO_3 \qquad \text{Reaction (3)}$$

$$H_2CO_3 \rightleftharpoons HCO_3^- + H^+ \qquad \text{Reaction (4)}$$

Given the instability of pH of DMEM solutions outside the incubator, a change in the protocol was required and a titration like experiment was made. The pH of cell medium was adjusted by adding step by step small volumes of acid or base as the pH was being measured by a standard probe and, simultaneously, the potential was being recorded using the iridium oxide-based pH probe.

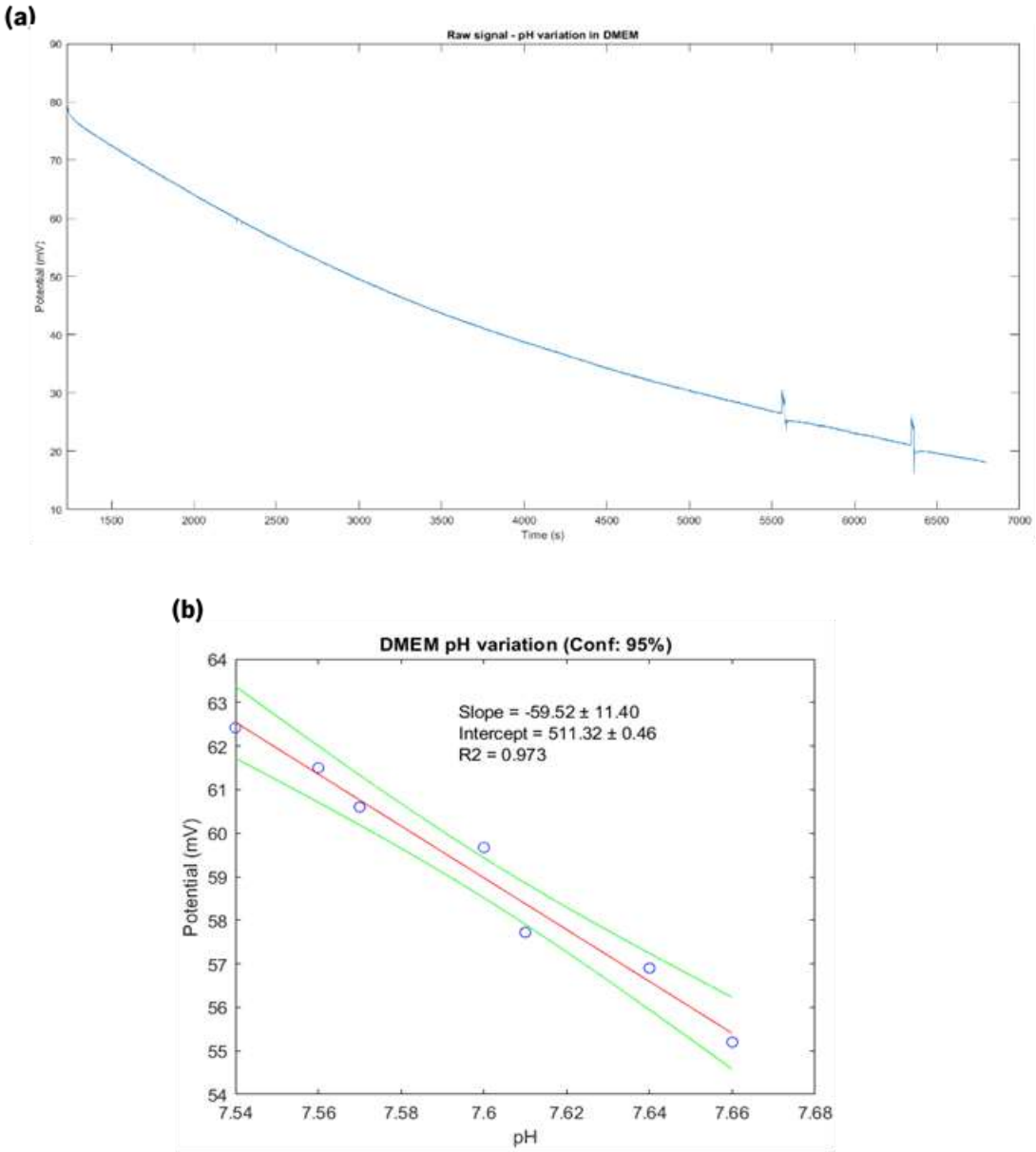

Figure 15. Raw signal measured the in-house-made electronic interface for titanium with IrOx and Nafion coating sensor in DMEM, over time (a) and respective calibration (potential vs pH) (b)

Using this new approach towards the calibrations in DMEM, the experiment for a titanium sensor not coated with Nafion was repeated and a sensitivity of -64.52 mV/pH was obtained, with an uncertainty of 3.04, a much smaller error than the ones determined previously (Figure S2).

Thereupon, another multiplexing experiment followed, where three replicas of this type of sensors were tested for a 7-day period. Initial calibrations were made at room temperature, then the electrodes were kept in the fridge, dipped in cell medium, so they could be further tested in 30 min recordings to check the stability of them throughout the defined period. Calibrations were repeated at the end of the experiment to evaluate if the sensors sensitivity had suffered alterations.

A careful analysis indicated that the errors were higher than anticipated, with the third sensor having the worst performance with a slope uncertainty of 11.29. Once again, the sensitivities were within the expected range and they did not change significantly after the 7-day period, confirmed by the overlapping of the error bars in figure 16a. In contrast, the intercept values were statistically different between replicas and between conditions (before and after 7 days). The fact that electrodes can maintain its sensitivity values showed the possibility of using the same sensors for recordings in cell culture up to 7 days.

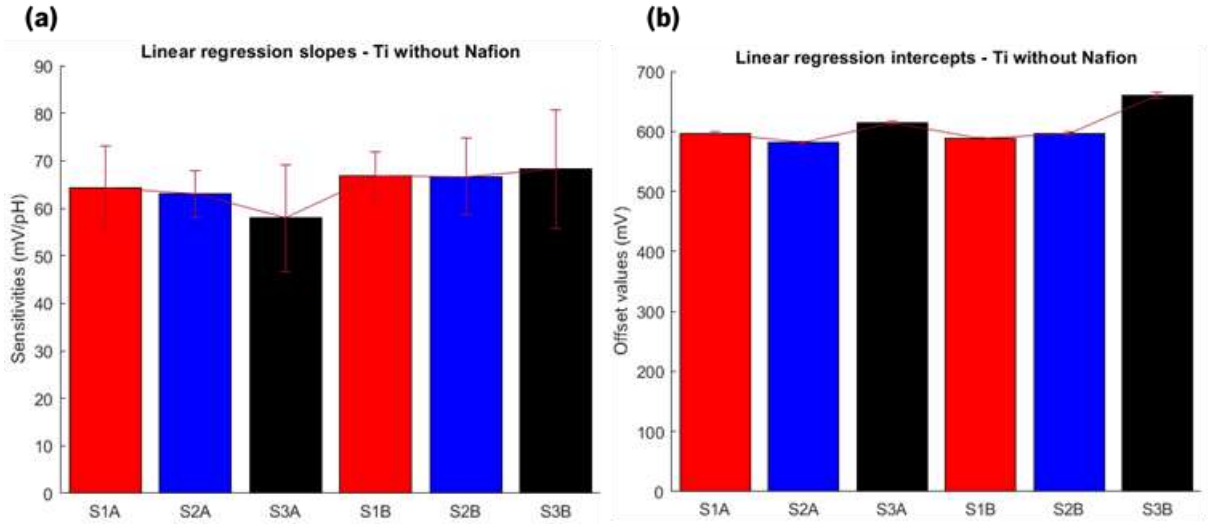

Figure 16. Comparison between the slopes obtained for each sensor before (SA) and after (SB) the 7-days period (a) and the intercepts (b)

As referred previously, the sensors stability in DMEM was tested for short periods of 30 minutes each for 4 days during the week the experiment ran. Initially, the pH of the medium was measured in the beginning, followed by the recording of the potential variations for 30 minutes, and finally, remeasuring the pH at the end of the 30 minutes. The results obtained are presented in table 1. The potential fluctuations observed were very high in some of the days recorded and, probably, caused by pH variations, as observed by recording pH at time zero and after thirty minutes, but they could also be attributed to changes in temperature, since the measurements were performed in environments in which these variables were not controlled (room temperature).

	SENSOR 1			
Recording days	Initial pH (t=0 min)	Final pH (t=30 min)	Average Potential (mV)	Drift (mV/min)
1°day	7.37	7.44	115.45	-0.066
2°day	7.70	7.18	97.77	-0.432
3°day	6.95	7.03	125.19	0.0078
4°day	7.27	7.32	108.00	-0.09
	SENSOR 2			
1°day	7.44	7.52	114.44	-0.15
2°day	7.68	7.94	91.82	-0.114
3°day	7.03	7.08	134.65	0.0408
4°day	7.32	7.38	111.87	0.0138
	SENSOR 3			
1°day	7.52	7.61	168.16	-0.0552
2°day	6.94	6..91	145.53	-0.084
3°day	7.08	7.14	179.17	0.12
4°day	7.38	7.40	158.15	-0.132

Table 1 - Drifts calculated for 30 minutes intervals in for 4 days during the span of a week and the respective initial and final pHs of the solutions tested

To determine if pH instability was the cause of the elevated drifts calculated we correlated the data by calculating the ratio between potential and pH changes - (Final potential value – Initial potential value)/(Final pH value – Initial pH value). The results were plotted according with the respective recording day, and we could conclude that there was some tendency for the ratios to follow a Nernstian behaviour, despite the existence of outliers (Figure 17). The random values may be attributed to temperature variations, instead of pH instability.

This experiment served the purpose of discovering if the sensors would behave differently after a long period of time and to further understand the instability of pH of DMEM in non-controlled environments.

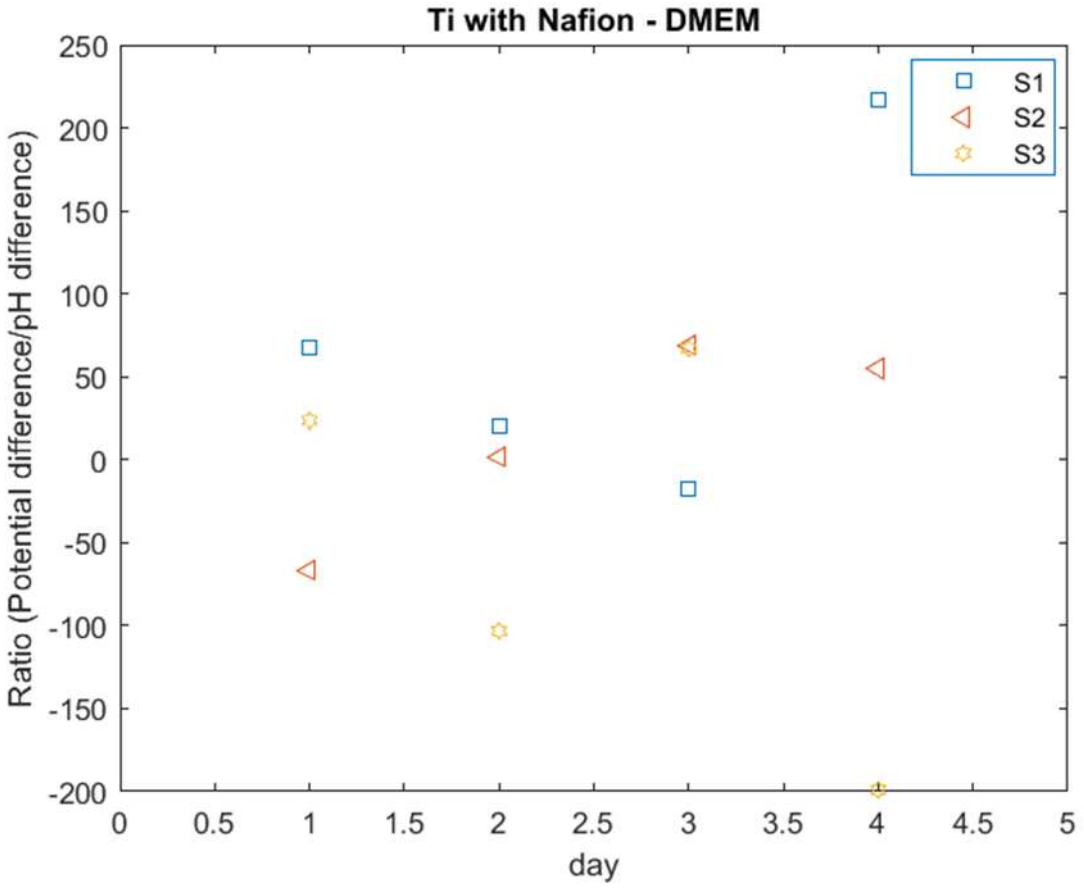

Figure 17. Potential changes per pH unit, during the 30 min recording in each of the 4 days, for each

4.3. Testing of a new reference electrode

So far, all the experiments were performed using a Ag/AgCl pseudo-reference electrode. This type of electrode lacks an inner filling solution to keep the concentration of Cl^- constant, and consequently, the electrode potential. The stability of the voltage difference and the pH measurements depends on the stability of the reference electrodes potential, as it does on pH sensing electrode. If this stability is affected, it causes drifting of the signal, affecting the accuracy of the obtained results. Therefore, the issue was tackled by constructing a simplistic reference electrode in which the Ag/AgCl electrode is immersed in a KCl inner filling solution (3M) and separated from the sample through a junction made of alginate embedded in a cotton structure (Figure 18).

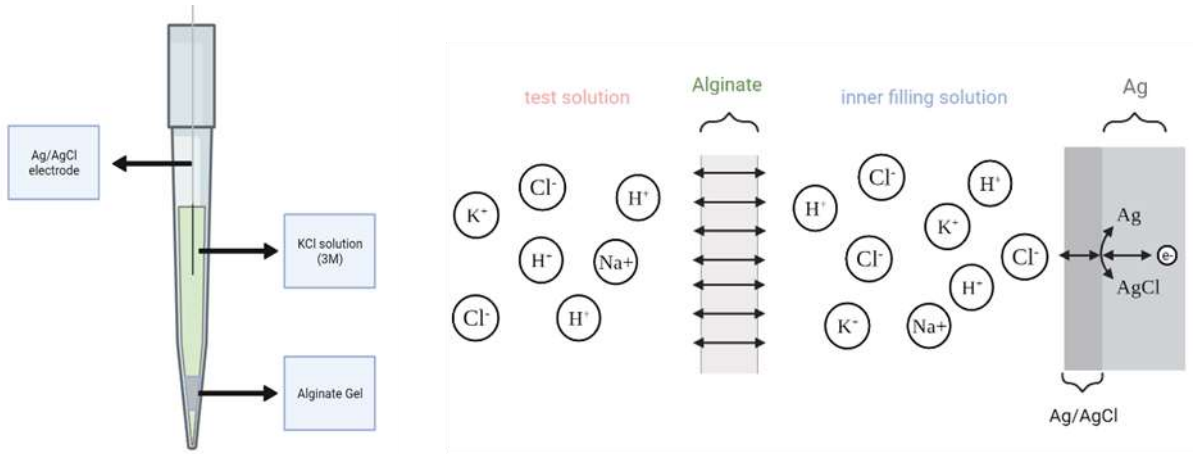

Figure 18. Schematic representation of the Reference Electrode

The drift - defined as slow variation of the output voltage of the sensing electrode as a function of time in a constant solution - associated with the reference electrode increases the error of calibrations, affecting the sensors accuracy (35). Thus, the performance of this new reference electrode was tested against a commercial Ag/AgCl reference electrode (part number: 6.0726.107, from Metrohm) and compared against the performance of the Ag/AgCl pseudo-reference, which had been used until this point. This evaluation was conducted in the PBS solution.

The data recorded was reduced for an average result, per minute (green line) and per hour (red line), represented in figure 19a and 19c. Afterwards, the reduced data was used to calculate the drift as a function of time, plotting it in a graph, and determining the average drift (Figures 19b and 19d). The drift was calculated by determining the slope of linear fit performed to the data set.

The signal was recorded over a period of approximately four days. The average drift obtained for the pseudo-reference was 0.0161 mV/h, an equivalent to 0.386 mV per day. In contrast, the reference electrode had an average drift of -0.0097 mV/h, which corresponds to 0.233 mV per day, confirming that the drift of the new reference electrode is smaller than the pseudo-reference.

Even though these results seemed promising, the reference electrodes had a lifetime of approximately a week or less before the leaking of the KCl solution began. The breaking of the barrier may be due to the lack of structural support of the cotton. Given the robust methodology behind the preparation of such electrodes, some sensors might have a more solid alginate junction, causing the variability. It is also

possible that the barrier maybe be disrupted by the insertion of the Ag/AgCl wire during the handling, inducing certainly leaking over time.

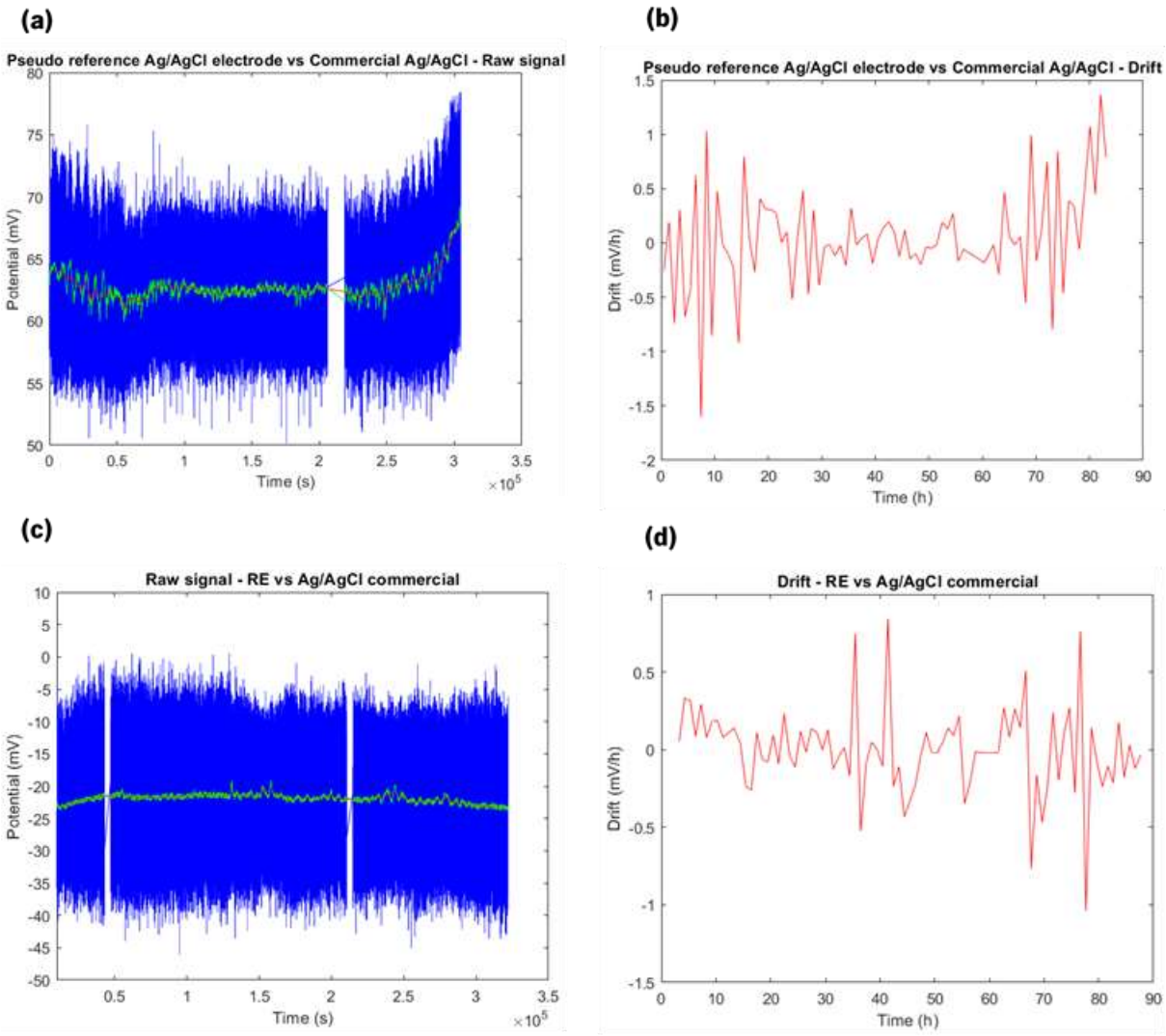

Figure 19. Raw signal and drift variation for the pseudo-reference electrode against the Ag/AgCl commercial electrode (a), (b) and raw signal and drift variation for the reference against the Ag/AgCl commercial electrode (c), (d), respectively

With such results, the next step consisted of testing the titanium with Nafion coating sensors, at room temperature, using the newly tested reference electrode. The high sensitivities were, again, consistent with the literature and the errors associated with both slopes and intercepts were smaller when compared to the ones obtained using the pseudo-reference electrode. It is important to note that sensors 2 and 3 were used with the same reference electrode, which reduces, consequently, the variability between these two replicas (Figure 20a).

4.4. Testing of the sensors in DMEM - different temperatures

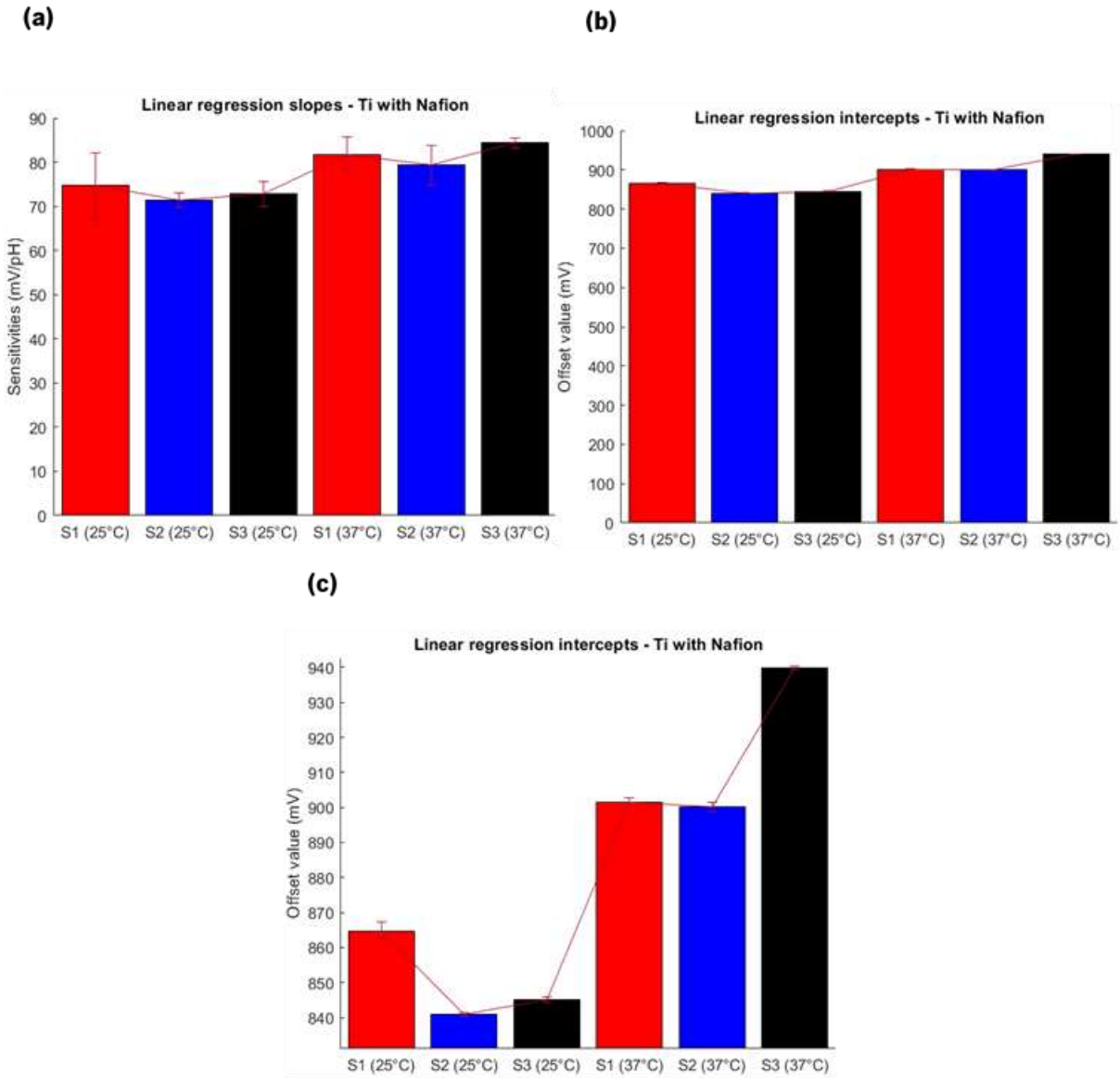

Figure 20. Comparison between the slopes obtained for each sensor at 25°C and at 37°C (a) and the intercepts (b). Amplified view of the intercepts bar chart (c)

The next step consisted in the continuation of calibrations, but at different temperature conditions. As deducted from the Nernst equation, the increase of temperature results in the increase of slope, and thus, an increase in the sensors sensitivity. In the results obtained an increase of the sensors sensitivity was found, as predicted by Nernst equation, and the uncertainty values were kept reduced by continuing with the titration protocol approach (Figure 21).

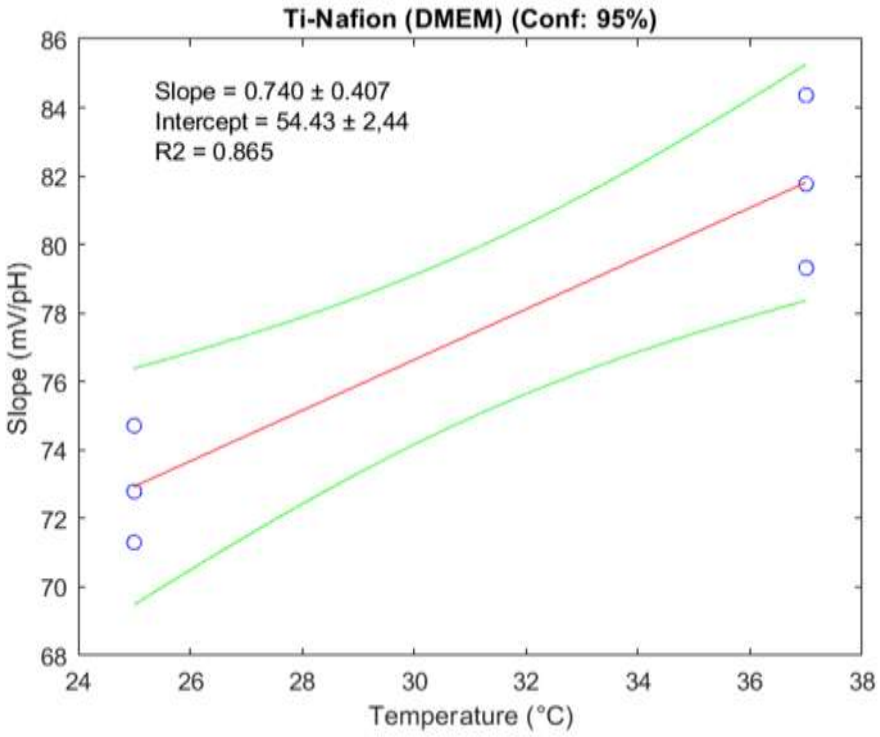

Figure 21. Correlation between sensitivities obtained at 25°C and at 37°C

According with the Nernst equation for 25°C, the potential changes -59.1 mV per pH unit, while at 37°C, this change increases to -61.5 mV per pH unit. We cannot compare these values to the ones we obtained, since these are considered for sensors following Nernstian behaviour, while our sensors sensors, normally present a super-Nernstian response. Having that in consideration, we analysed the correlation between sensitivities and temperature. For the sensitivities of -59.1 mV/pH and -61.5, we determined a slope of, approximately, 0.2 mV/pH.°C. By performing a linear regression using our data set, we concluded that our slope is 0.7 mV/pH.°C, which is a lot superior to what would be expected (Figure 21).

Considering the main goal resides in using the measured potential values to determined samples pH, it becomes necessary to invert the variables in the linear regressions, representing the data pH vs potential. The linear regression model allows for the uncertainty calculation of both slope and intercept, and thus, the uncertainty associated to pH variation per mV unit was determined by switching the parameters in the original calculation. This uncertainty was always smaller than 0.001 pH units per mV, what is ideal for the pH range of 1 pH unit used in these studies (Figure 22).

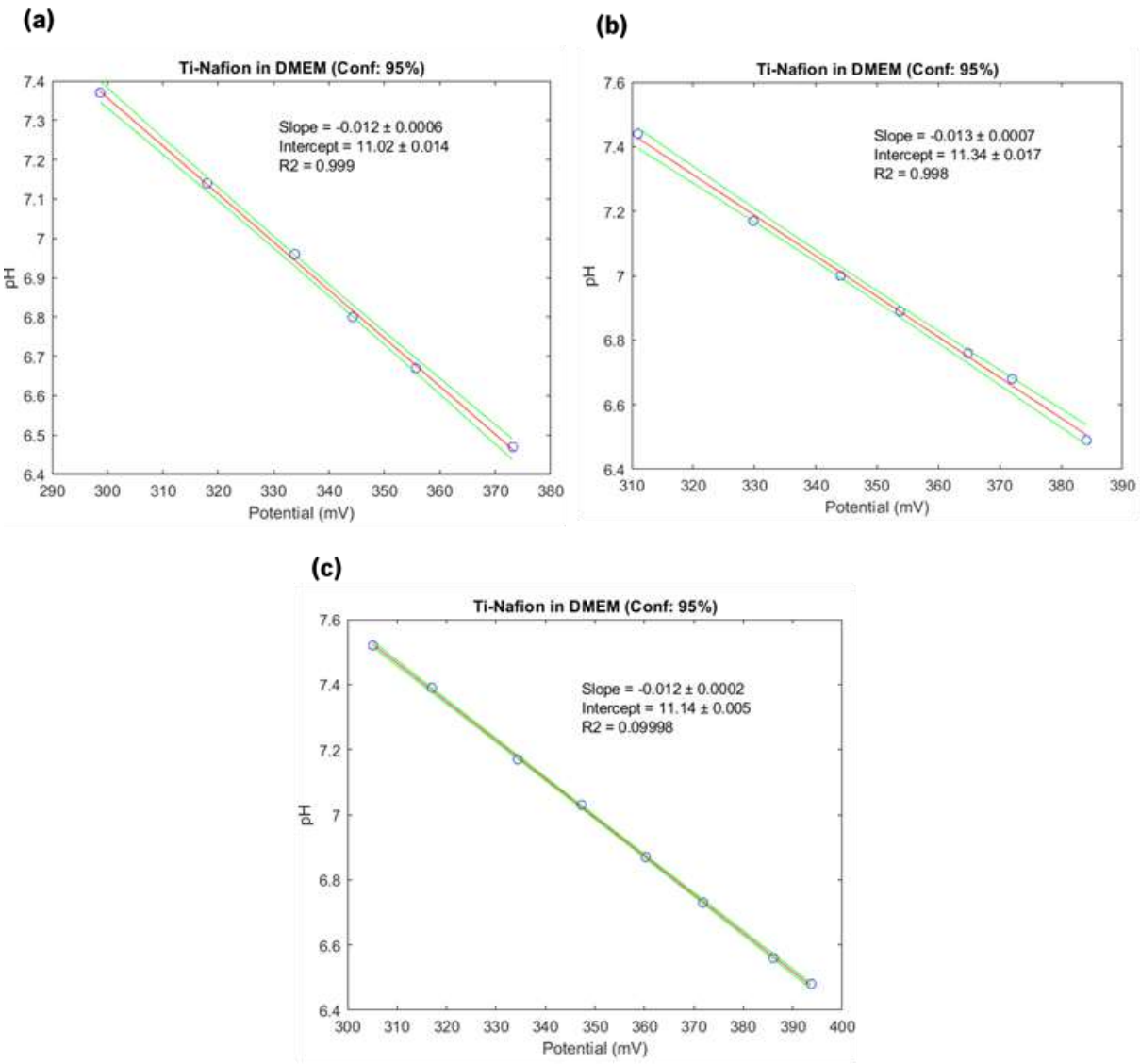

Figure 22. Calibrations (pH vs potential) using the values measured in DMEM by the new in-house-made electronic interface for titanium with IrOx and Nafion coated sensors 1 (a), 2 (b) and 3 (c), at 37 °C

Another interesting observation made while testing sensors coated with Nafion was the change observed in the potential range when comparing them with the sensors without coating. Nafion is a polymer composed of a polytetrafluoroethylene (PTFE) backbone with perfluorinated-vinyl-polyether side chains which contain sulphonic acid end groups. This acidic group contributes for the high proton conductivity, through the Grotthuss mechanism, but it can also cause the increase of potential range of the sensors with this layer, due to locally higher acidity.

4.5. pH sensor performance

There are several characteristics, which define the performance of pH sensors. Stability, response time, selectivity, interference of other ions, hysteresis and potential drift are the conventional parameters, that are recurrently tested, when building a pH sensing system. More essential parameters may be added, depending on what is required from the pH sensor. If the pH sensor ought to be applied in cell culture environments, then there is a need for it to be biological compatible and resistant to the sterilization procedures.

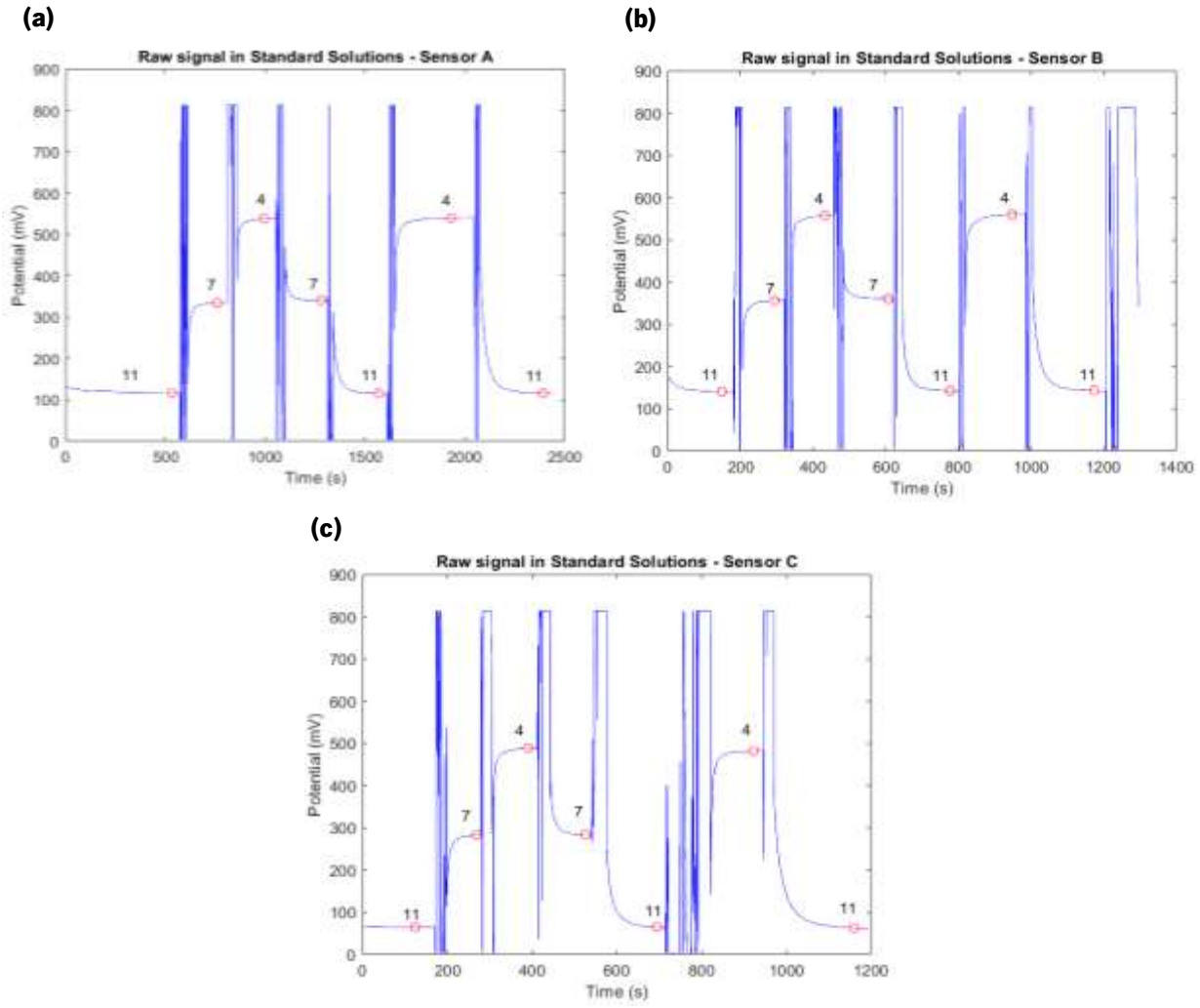

Figure 24. Raw signal of potential differences measured in the standard solutions with pH values 4, 7, 9 (as individualized on graph) by the new house-made electronic interface for titanium with IrOx and Nafion coating sensors A (a), B (b) and C (c), at room temperature

With the purpose of analysing the performance of the sensors a series of tests was conducted with the purpose of analysing electrodes sensitivity, reversibility, and reproducibility, in standard pH solutions (4, 7, 11).

First, three sensors (three replicas) were tested in the three standard solutions (4, 7, 11) and the potential values measured were used to make a fit and analysis (Figure 24). The calculated potential averages were used to calculate the sensors sensitivity and the slopes obtained were closer to the Nernst behaviour than the sensitivities of previous tests (-61.78, -63.48 and -62.12 mV/pH). It is likely that this sensitivity variability between different batches of electrodes is due to the differences of ratios between both iridium oxidation states in the deposited layer.

Given the extended range of pH values used, linear regression was not the proper fitting model to be applied. Hence, the data was fitted accordingly with the model of a polynomial function. After calculating the function, we derived it and used the derivative to calculate the slope in point 7, which would represent the sensitivity in the range we have been studying (Figure 25).

(a)

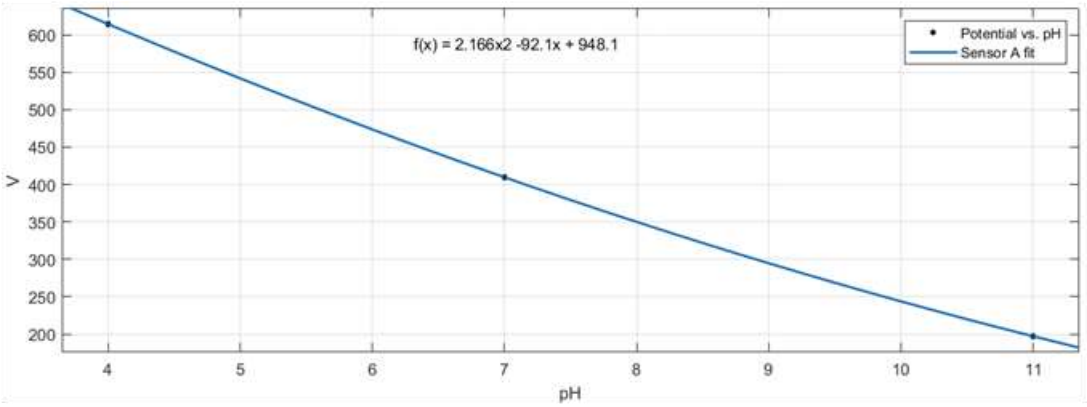

(b)

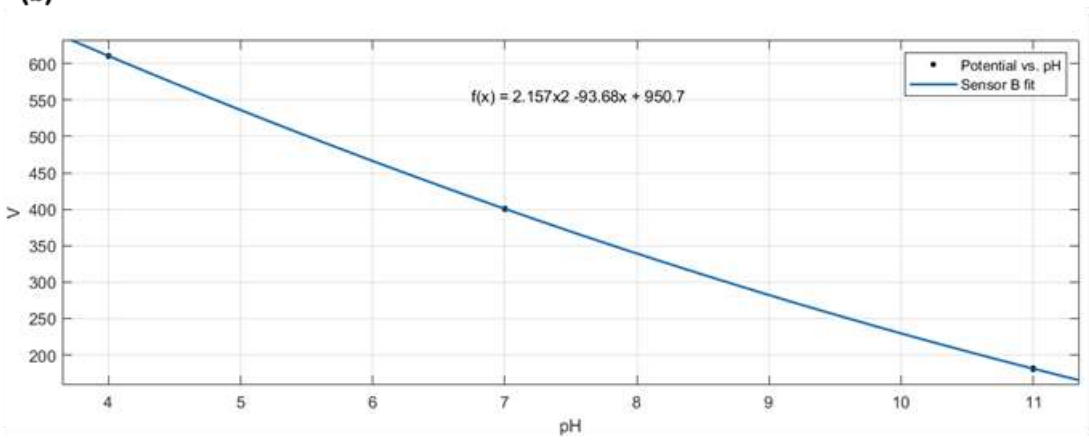

(c)

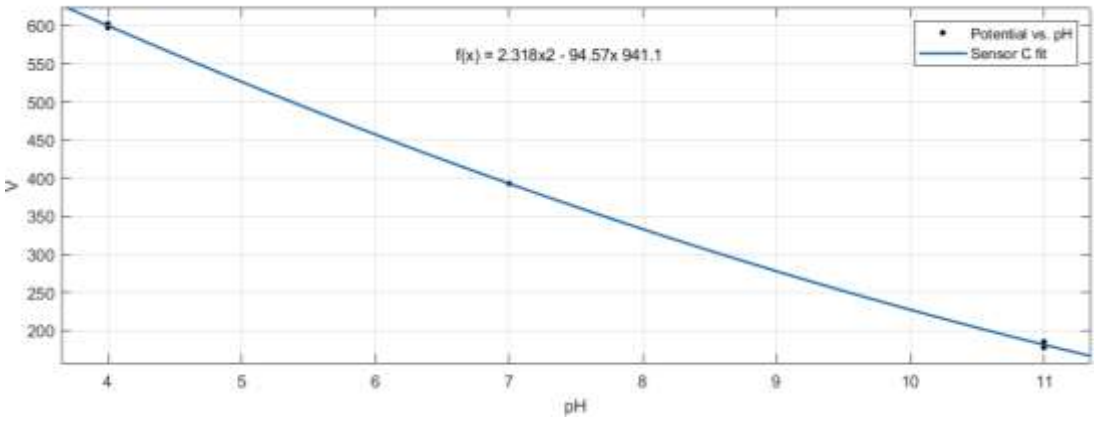

Figure 25. Polynomial fitting for sensors A (a), B (b) and C (c) from first measurements

When a pH electrode which has been used repeatedly in the same pH solution, it retains memory, which can lead to erroneous output potential values (35). To analyse the reversibility of the sensors, we calculated the differences between the potential values for pH value 7, from pH 11, 7 to 4 and back to 4, 7 and 11. These measurements in loop allow for the calculation of hysteresis. Sensor B was the one manifesting the higher hysteresis values (1.06 mV), which can be considered negligible (figure 26a).

After hysteresis was analysed, we proceeded to calculate the response times. This parameter exact definition varies throughout the literature, but it is conventionally designated as the time it takes for the electrodes potential to reach 90% of a stable value after its immersion in a new solution (35). This parameter importance depends on the application of the sensors. For this work, fast response times are not required, since are intended for long term cell culture monitoring. They were then determined resorting to two different methods: (1) change of pH from more basic solution to more acidic solution and (2) change of pH from more acidic solution to a more basic solution (53). The conclusion reached was that the response times varied depending on the method used, being the first method the one resulting in smaller response times (approximately 23 seconds) (Figure 26c).

Four weeks after these initial tests, these experiments were repeated to investigate if the performance of the sensing and reference electrodes was maintained or if there were significant differences, setting a clear time frame in which these sensors can be reused keeping the same accuracy.

It was observed that the sensitivities were not significantly different (overlap of the error bars), although there was an increase in uncertainty of the sensitivity of the sensors after the 4-week period (Figure 27). On the other hand, the reversibility capacity of the sensors decreased, with a maximum hysteresis value of 7.14 mV (Figure 24a). A decrease of performance of the sensors with time is predictable, however, the same was not observed for the response times. As previously, the second method presented the higher response times, nevertheless, after the 4 week-period, the response times decreased considerably, being the highest 18 seconds for the sensor A (Figure 26c). This result was unexpected and is contradictory to posterior tests made in PBS and DMEM solutions, where the stability of the raw signal manifested to be higher for older electrodes.

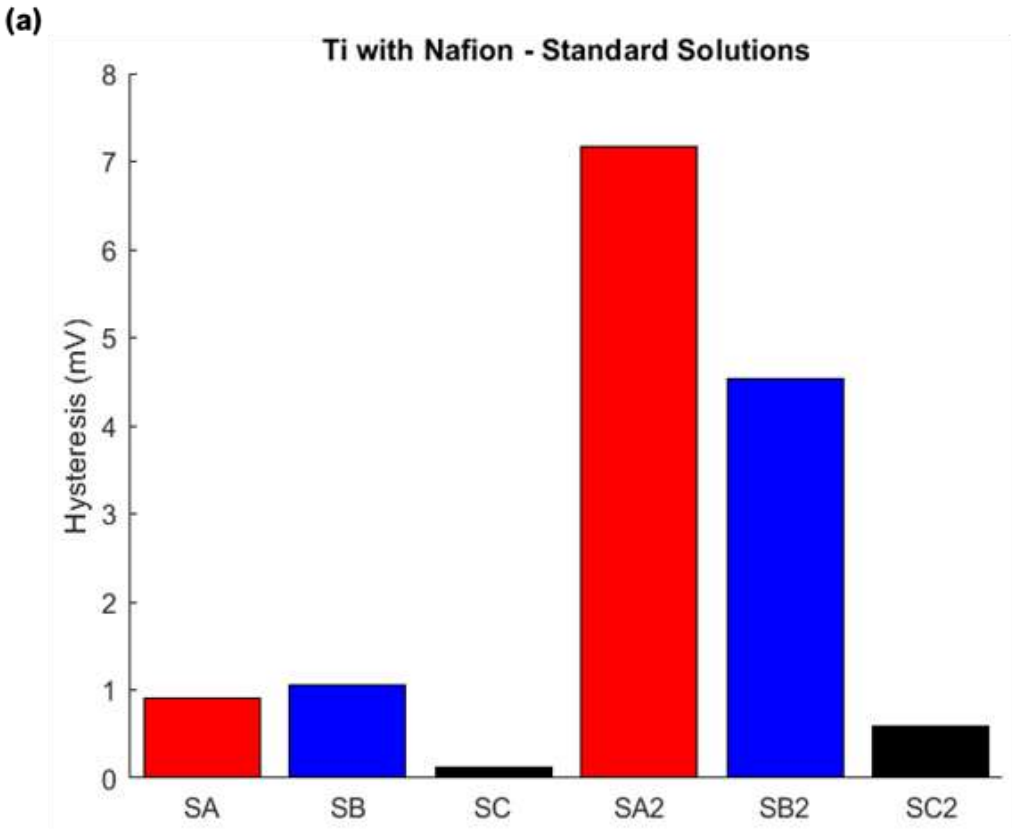

(b)

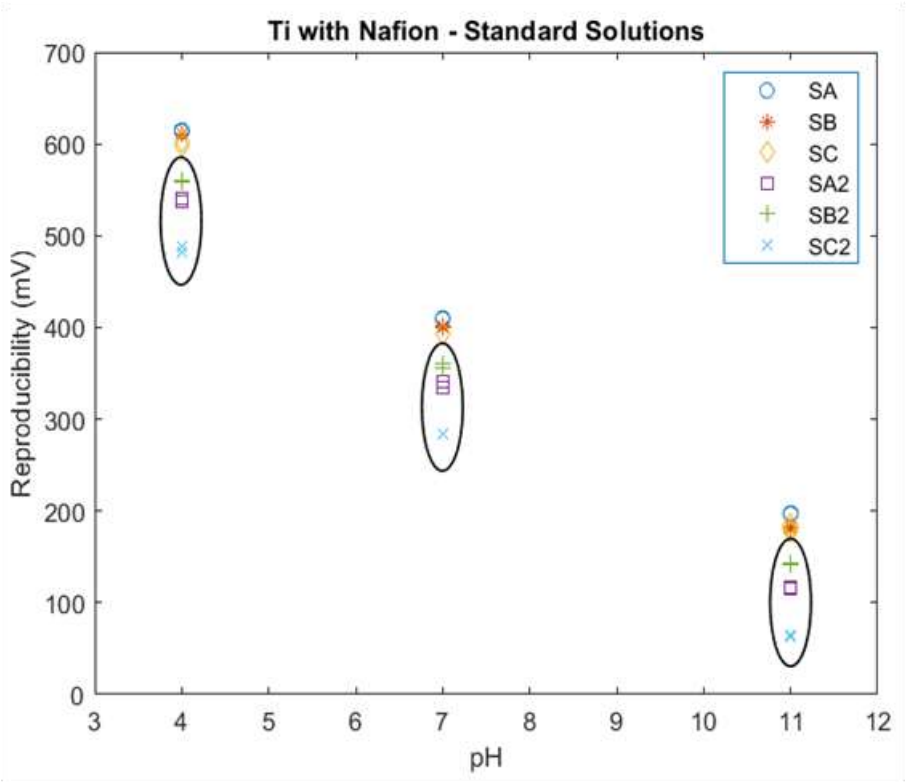

(c)

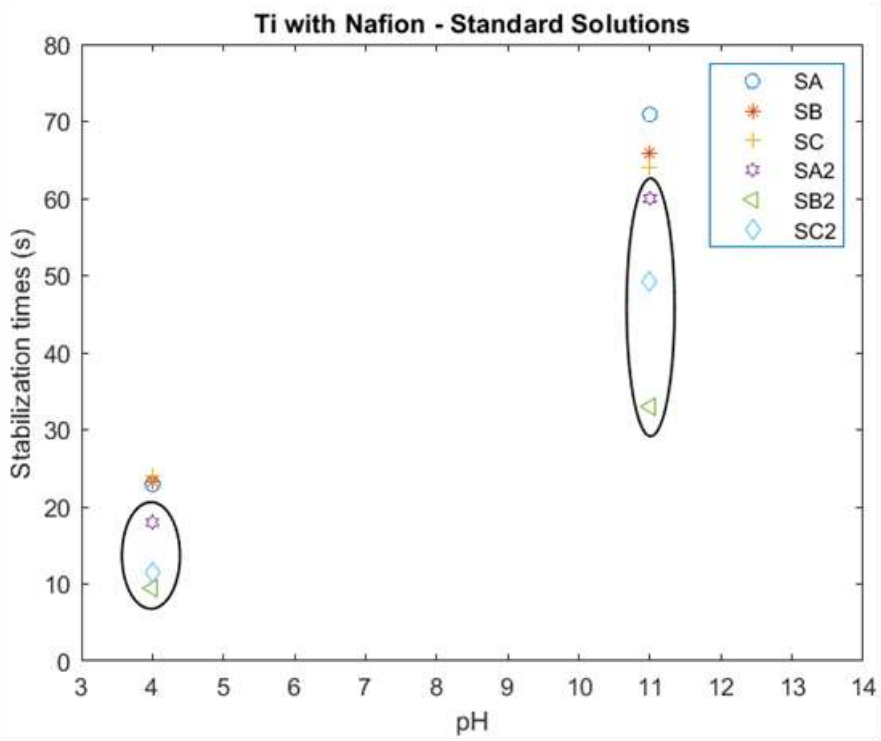

Figure 26. Performance of pH sensors in standard solutions (4, 7, 11) for different parameters: hysteresis (a), reproducibility (b), stabilization times (c), before and after a 4-week period. The ellipses around the data highlight the values measured after the 4-weeks period

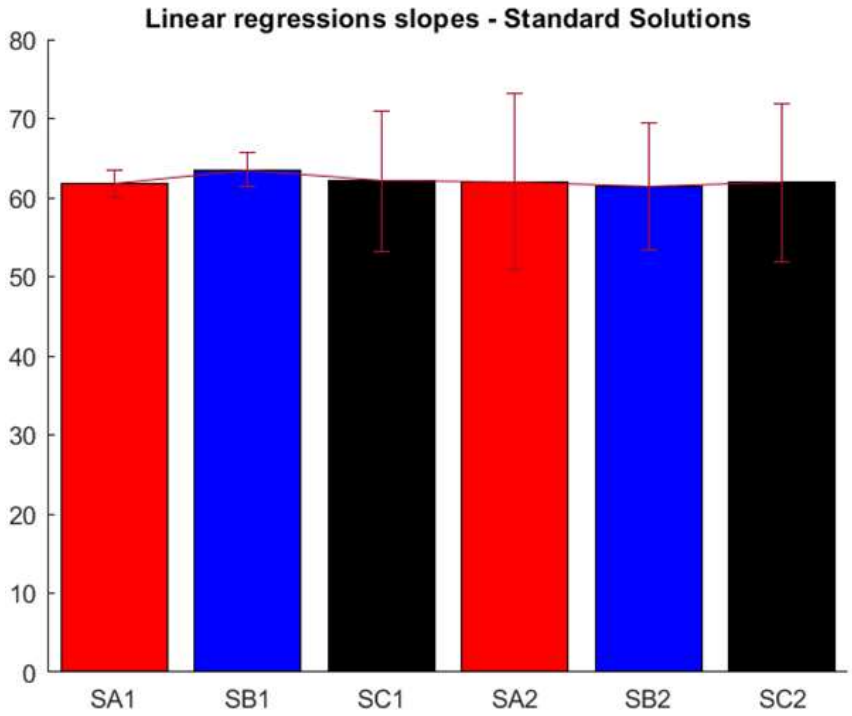

Figure 27. Comparison between the slopes obtained for each sensor before (S1) and after (S2) the 4-week period

4.6. Multiwell plate experiments

Initially, calibrations were made in PBS solutions with the purpose of confirming the slope obtained for each well, given that the previous calibrations were made using a different electronic system.

The sensors sensitivity remains above the Nernstian slope as expected, but not as higher as the ones obtained previously, since these calibrations were done at room temperature. The variability between each well set is not significant, since the slopes are similar. However, the error associated with the senso rs sets in wells 4 and 6 is a lot higher comparative with the other wells (Figure 28). Since the solutions used were buffer solutions, and th pH is expectedly stable, the decrease in reproducibility has been attributed to potential fluctuations of the reference electrode.

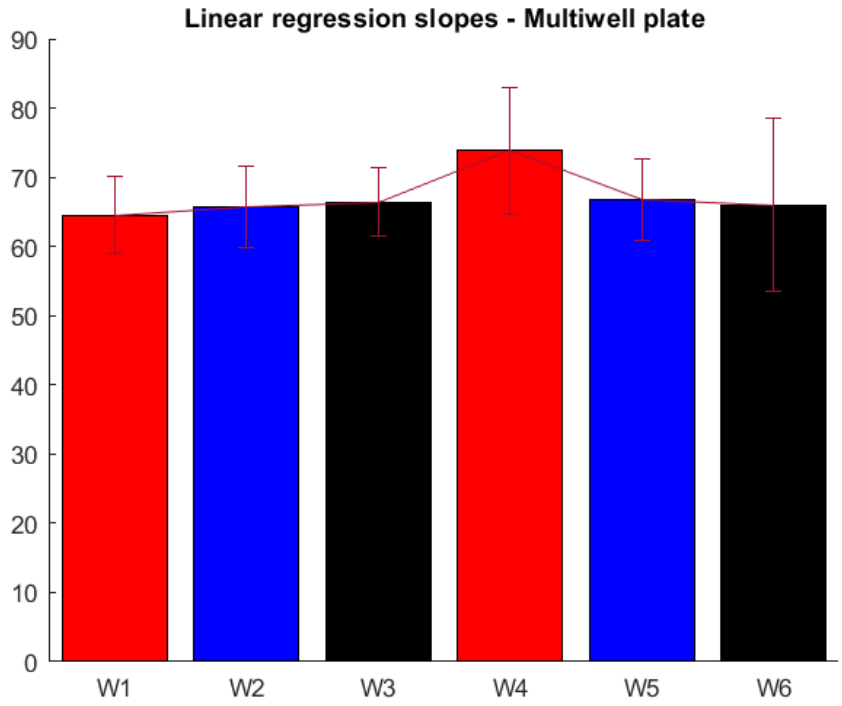

Figure 28. Comparison between the slopes obtained for sensors set correspondent to each well

4.7. Preliminary multiwell plate cell experiments

For the cell experiment in the multiwell plate two conditions were tested: three wells with MCF-7 cells and three wells with only cell medium. Considering the different conditions, we were expecting to observe a gradual Increase of potential over time in the wells cultured with cells, due to the continuous acidification of cell medium.

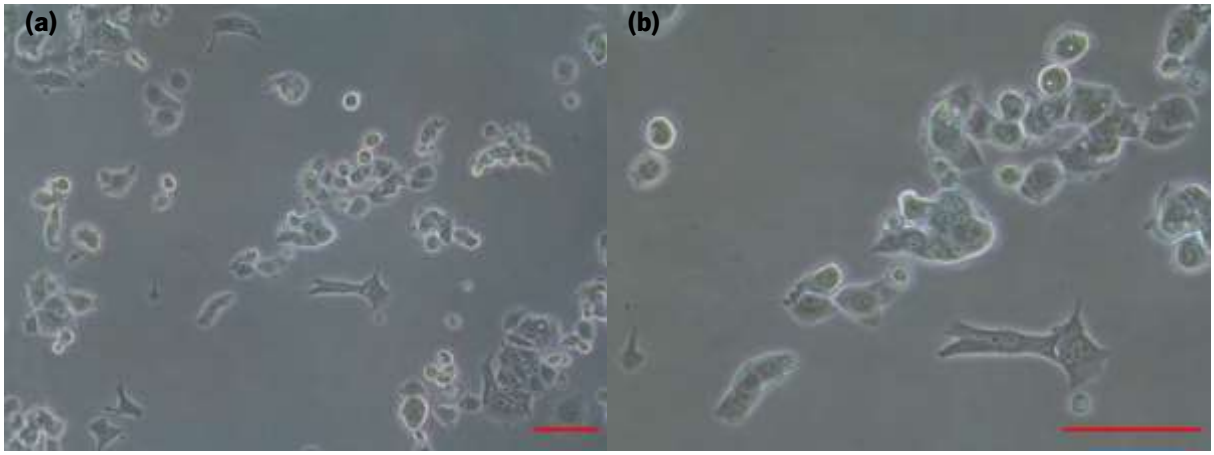

Figure 29. Optical microscopy images of MCF-7 cells at passage 7 growing in cell culture flasks. 10x (a) and 20x (b) magnification (scale bar – 100 µm)

An initial rise of potential in the control conditions were also expected due to the initial rise of the medium pH due to the CO_2 percentage inside the incubator. With the passing of days, the potential signal for the wells with cells would be higher compared with the control conditions. However, we did not observe such a change in potential as the cells grew. At t=10h, when the signal was already stable, there is not a clear distinction between test conditions and controls. Two of the wells with the cells manifested a smaller potential value than control conditions. Throughout the 3 days of testing, the cells metabolization wasn't observed in the potential signal. And for three of the wells (two controls and one with test condition) there was a drastic increase of potential, followed by a slow decrease of it during the following days (Figure 30). The reason for the anomalous output values is unclear. We assume, at this stage, they it could have been due to some disconnection between electrodes and interface, or even because the active area of the electrode stopped being in contact with the medium.

As such, the experiment had to be terminated, and we could not proceed with it and confirm if with more days passed, the expected potential variations would be seen.

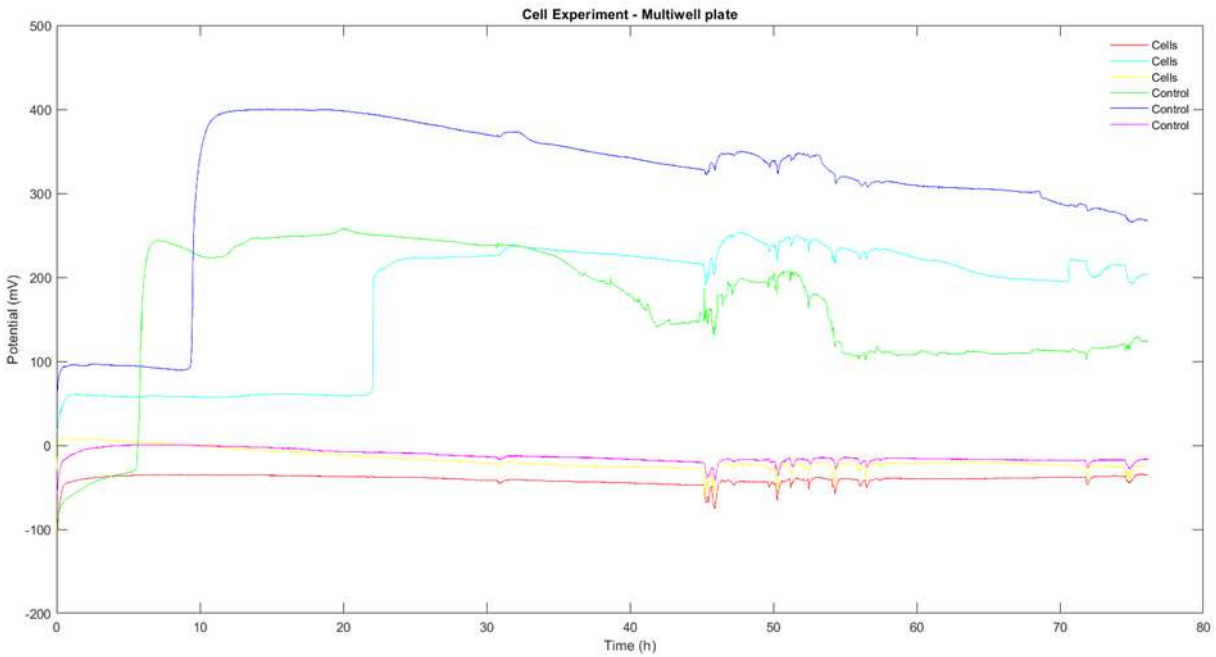

Figure 30. Raw signal of the multiwell experiment with MCF-7 cell line in the wells and three controls

5. Conclusion remarks and future perspectives

The optimized electrochemical sensing system manifested the expected high sensitivity and accuracy as described in the literature, and it has been optimized for the application in cell culture systems, where the pH changes are very reduced, with a maximum of pH change of one pH unit. However, some concerns persist regarding the reference electrode. Despite being stable for long periods of time, the reference electrode with the inner filling solution revealed leaking issues that proved to interfere with the voltage signal leading to random output values. This enhances the need of replacing the used reference electrode by a more efficient alternative, which fixes the leaking problems presented.

Provided the difficulties encountered throughout calibration experiments, it is also taken in consideration the use of cell medium without carbonate-based buffering systems. This allows for experiments to be run simplistically in non-controlled CO_2 environments, without causing pH instability of the tested solutions.

Furthermore, the developed pH sensing system should continue to be tested in the designed 2D cell culture system once the reference electrode issue is resolved and, posteriorly be integrated in the bioreactor developed for the project main purpose.

References

1. Breslin S, O'Driscoll L. Three-dimensional cell culture: The missing link in drug discovery. Drug Discov Today. 2013;18(5–6):240–9. Available from: http://dx.doi.org/10.1016/j.drudis.2012.10.003

2. Langhans SA. Three-Dimensional in Vitro Cell Culture Models in Drug Discovery and Drug Repositioning. Front Pharmacol. 2018;9(JAN):1–14. Available from: http://journal.frontiersin.org/article/10.3389/fphar.2018.00006/full

3. Caballero D, Kaushik S, Correlo VM, Oliveira JM, Reis RL, Kundu SC. Organ-on-chip models of cancer metastasis for future personalized medicine: From chip to the patient. Biomaterials. 2017 Dec;149:98–115. Available from: https://linkinghub.elsevier.com/retrieve/pii/S014296121730635X

4. Alemany-Ribes M, Semino CE. Bioengineering 3D environments for cancer models. Adv Drug Deliv Rev. 2014;79:40–9. Available from: http://dx.doi.org/10.1016/j.addr.2014.06.004

5. Kim S, Lee H, Chung M, Jeon NL. Engineering of functional, perfusable 3D microvascular networks on a chip. Lab Chip. 2013;13(8):1489. Available from: http://xlink.rsc.org/?DOI=c3lc41320a

6. Moshksayan K, Kashaninejad N, Warkiani ME, Lock JG, Moghadas H, Firoozabadi B, et al. Spheroids-on-a-chip: Recent advances and design considerations in microfluidic platforms for spheroid formation and culture. Sensors Actuators, B Chem. 2018;263(January):151–76. Available from: http://dx.doi.org/10.1016/j.snb.2018.01.223

7. van Duinen V, Trietsch SJ, Joore J, Vulto P, Hankemeier T. Microfluidic 3D cell culture: From tools to tissue models. Curr Opin Biotechnol. 2015;35:118–26. Available from: http://dx.doi.org/10.1016/j.copbio.2015.05.002

8. Whitesides GM. The origins and the future of microfluidics. Nature. 2006 Jul 26;442(7101):368–73. Available from: http://www.nature.com/articles/nature05058

9. Bhatia SN, Ingber DE. Microfluidic organs-on-chips. Nat Biotechnol. 2014 Aug 5;32(8):760–72. Available from: http://www.nature.com/articles/nbt.2989

10. Wu Q, Liu J, Wang X, Feng L, Wu J, Zhu X, et al. Organ-on-a-chip: Recent breakthroughs and future prospects. Biomed Eng Online. 2020;19(1):1–19. Available from: https://doi.org/10.1186/s12938-020-0752-0

11. Mermoud Y, Felder M, Stucki JD, Stucki AO, Guenat OT. Microimpedance tomography system to monitor cell activity and membrane movements in a breathing lung-on-chip. Sensors Actuators, B Chem. 2018;255:3647–53. Available from: http://dx.doi.org/10.1016/j.snb.2017.09.192

12. Riahi R, Shaegh SAM, Ghaderi M, Zhang YS, Shin SR, Aleman J, et al. Automated microfluidic platform of bead-based electrochemical immunosensor integrated with bioreactor for continual monitoring of cell secreted biomarkers. Sci Rep. 2016;6(March):1–14. Available from: http://dx.doi.org/10.1038/srep24598

13. Mastikhina O, Moon BU, Williams K, Hatkar R, Gustafson D, Mourad O, et al. Human cardiac fibrosis-on-a-chip model recapitulates disease hallmarks and can serve as a platform for drug testing. Biomaterials. 2020;233(August 2019):119741. Available from: https://doi.org/10.1016/j.biomaterials.2019.119741

14. Du Y, Khandekar G, Llewellyn J, Polacheck W, Chen CS, Wells RG. A Bile Duct-on-a-Chip With Organ-Level Functions. Hepatology. 2020 Apr 28;71(4):1350–63. Available from: https://onlinelibrary.wiley.com/doi/10.1002/hep.30918

15. Jalili-Firoozinezhad S, Gazzaniga FS, Calamari EL, Camacho DM, Fadel CW, Bein A, et al. A complex human gut microbiome cultured in an anaerobic intestine-on-a-chip. Nat Biomed Eng. 2019 Jul 13;3(7):520–31. Available from: http://www.nature.com/articles/s41551-019-0397-0

16. Yin F, Zhu Y, Zhang M, Yu H, Chen W, Qin J. A 3D human placenta-on-a-chip model to probe nanoparticle exposure at the placental barrier. Toxicol Vitr. 2019;54(June 2018):105–13. Available from: https://doi.org/10.1016/j.tiv.2018.08.014

17. Essaouiba A, Okitsu T, Kinoshita R, Jellali R, Shinohara M, Danoy M, et al. Development of a pancreas-liver organ-on-chip coculture model for organ-to-organ interaction studies. Biochem Eng J. 2020;164(August):1–11.

18. Huh D, Leslie DC, Matthews BD, Fraser JP, Jurek S, Hamilton GA, et al. A human disease model of drug toxicity-induced pulmonary edema in a lung-on-a-chip microdevice. Sci Transl Med. 2012;4(159):1–5.

19. Oleaga C, Bernabini C, Smith AST, Srinivasan B, Jackson M, McLamb W, et al. Multi-Organ toxicity demonstration in a functional human in vitro system composed of four organs. Sci Rep. 2016;6(December 2015):1–17. Available from: http://dx.doi.org/10.1038/srep20030

20. Fontoura JC, Viezzer C, dos Santos FG, Ligabue RA, Weinlich R, Puga RD, et al. Comparison of 2D and 3D cell culture models for cell growth, gene expression and drug resistance. Mater Sci Eng C. 2020;107(September 2019):1–10. Available from: https://doi.org/10.1016/j.msec.2019.110264

21. Sobrino A, Phan DTT, Datta R, Wang X, Hachey SJ, Romero-López M, et al. 3D microtumors in vitro supported by perfused vascular networks. Sci Rep. 2016;6(August):1–11. Available from: http://dx.doi.org/10.1038/srep31589

22. Hao S, Ha L, Cheng G, Wan Y, Xia Y, Sosnoski DM, et al. A Spontaneous 3D Bone-On-a-Chip for Bone Metastasis Study of Breast Cancer Cells. Small. 2018 Mar;14(12):1–10. Available from: https://onlinelibrary.wiley.com/doi/10.1002/smll.201702787

23. Skardal A, Devarasetty M, Forsythe S, Atala A, Soker S. A reductionist metastasis-on-a-chip platform for in vitro tumor progression modeling and drug screening. Biotechnol Bioeng. 2016;113(9):2020–32.

24. Steinegger A, Wolfbeis OS, Borisov SM. Optical Sensing and Imaging of pH Values: Spectroscopies, Materials, and Applications. Chem Rev. 2020 Nov 25;120(22):12357–489. Available from: https://pubs.acs.org/doi/10.1021/acs.chemrev.0c00451

25. Jensen FB. Red blood cell pH, the Bohr effect, and other oxygenation-linked phenomena in blood O2 and CO2 transport. Acta Physiol Scand. 2004 Nov;182(3):215–27. Available from: https://onlinelibrary.wiley.com/doi/10.1111/j.1365-201X.2004.01361.x

26. Aoi W, Marunaka Y. Importance of pH Homeostasis in Metabolic Health and Diseases: Crucial Role of Membrane Proton Transport. Biomed Res Int. 2014;2014:1–8. Available from: http://www.hindawi.com/journals/bmri/2014/598986/

27. Counihan JL, Grossman EA, Nomura DK. Cancer Metabolism: Current Understanding and

Therapies. Chem Rev. 2018 Jul 25;118(14):6893–923. Available from: https://pubs.acs.org/doi/10.1021/acs.chemrev.7b00775

28. DeBerardinis RJ, Chandel NS. Fundamentals of cancer metabolism. Sci Adv. 2016 May 27;2(5):1–18. Available from: https://www.science.org/doi/10.1126/sciadv.1600200

29. J Akhenblit P, D Pagel M. Recent Advances in Targeting Tumor Energy Metabolism with Tumor Acidosis as a Biomarker of Drug Efficacy. J Cancer Sci Ther. 2016;08(01):20–9. Available from: https://www.omicsonline.org/open-access/recent-advances-in-targeting-tumor-energy-metabolism-with-tumoracidosis-as-a-biomarker-of-drug-efficacy-1948-5956-1000382.php?aid=67758

30. Teoh ST, Lunt SY. Metabolism in cancer metastasis: bioenergetics, biosynthesis, and beyond. Wiley Interdiscip Rev Syst Biol Med. 2018 Mar;10(2):e1406. Available from: https://onlinelibrary.wiley.com/doi/10.1002/wsbm.1406

31. Zhang X, Lin Y, Gillies RJ. Tumor pH and Its Measurement. J Nucl Med [Internet]. 2010 Aug;51(8):1167–70. Available from: http://jnm.snmjournals.org/lookup/doi/10.2967/jnumed.109.068981

32. Li Y, Wang Y, Yang S, Zhao Y, Yuan L, Zheng J, et al. Hemicyanine-based High Resolution Ratiometric near-Infrared Fluorescent Probe for Monitoring pH Changes in Vivo. Anal Chem. 2015 Feb 17;87(4):2495–503. Available from: https://pubs.acs.org/doi/10.1021/ac5045498

33. Wu W, Shen J, Banerjee P, Zhou S. Chitosan-based responsive hybrid nanogels for integration of optical pH-sensing, tumor cell imaging and controlled drug delivery. Biomaterials. 2010;31(32):8371–81. Available from: http://dx.doi.org/10.1016/j.biomaterials.2010.07.061

34. Buck RP, Rondinini S, Covington AK, Baucke FGK, Brett CMA, Camoes MF, et al. Measurement of pH. Definition, standards, and procedures (IUPAC Recommendations 2002). Pure Appl Chem. 2002 Jan 1;74(11):2169–200. Available from: https://www.degruyter.com/document/doi/10.1351/pac200274112169/html

35. Manjakkal L, Szwagierczak D, Dahiya R. Metal oxides based electrochemical pH sensors: Current progress and future perspectives. Prog Mater Sci. 2020 Apr;109(December 2019):1–31. Available from: https://doi.org/10.1016/j.pmatsci.2019.100635

36. Skoog DA, Holler FJ, Crouch SR. Principles of Instrumental Analysis. 6th ed. ThomsonBrooks/Cole; 2007.

37. Kurzweil P. Metal Oxides and Ion-Exchanging Surfaces as pH Sensors in Liquids: State-of-the-Art and Outlook. Sensors. 2009 Jun 23;9(6):4955–85. Available from: http://www.mdpi.com/1424-8220/9/6/4955

38. Syu Y-C, Hsu W-E, Lin C-T. Review—Field-Effect Transistor Biosensing: Devices and Clinical Applications. ECS J Solid State Sci Technol. 2018 Jun 13;7(7):Q3196–207. Available from: https://iopscience.iop.org/article/10.1149/2.0291807jss

39. Lee C-S, Kim S, Kim M. Ion-Sensitive Field-Effect Transistor for Biological Sensing. Sensors. 2009 Sep 7;9(9):7111–31. Available from: http://www.mdpi.com/1424-8220/9/9/7111

40. Hu J, Stein A, Bühlmann P. Rational design of all-solid-state ion-selective electrodes and reference electrodes. TrAC - Trends Anal Chem. 2016;76:102–14. Available from: http://dx.doi.org/10.1016/j.trac.2015.11.004

41. Yoshinobu T, Miyamoto K, Werner CF, Poghossian A, Wagner T, Schöning MJ. Light-Addressable Potentiometric Sensors for Quantitative Spatial Imaging of Chemical Species. Annu Rev Anal Chem. 2017 Jun 12;10(1):225–46. Available from: https://www.annualreviews.org/doi/10.1146/annurev-anchem-061516-045158

42. GES I, IVANOV B, SCHAFFER D, LIMA E, WERDICH A, BAUDENBACHER F. Thin-film IrO pH microelectrode for microfluidic-based microsystems. Biosens Bioelectron. 2005 Aug 15;21(2):248–56. Available from: https://linkinghub.elsevier.com/retrieve/pii/S0956566304004221

43. Olthuis W, Robben MAM, Bergveld P, Bos M, van der Linden WE. pH Sensor Properties of Electrochemically Grown Iridium Oxide. Sensors Actuators B Chem. 1990 Oct;2(4):247–56. Available from: https://linkinghub.elsevier.com/retrieve/pii/092540059080150X

44. Hitchman ML, Ramanathan S. Considerations of the pH dependence of hydrous oxide films formed on iridium by voltammetric cycling. Electroanalysis. 1992 Mar;4(3):291–7. Available from: https://onlinelibrary.wiley.com/doi/10.1002/elan.1140040306

45. Zhou B, Bian C, Tong J, Xia S. Fabrication of a Miniature Multi-Parameter Sensor Chip for Water Quality Assessment. Sensors. 2017 Jan 14;17(1):1–14. Available from: http://www.mdpi.com/1424-8220/17/1/157

46. Ng SR, O'Hare D. An iridium oxide microelectrode for monitoring acute local pH changes of endothelial cells. Analyst. 2015;140(12):4224–31. Available from: http://xlink.rsc.org/?DOI=C5AN00377F

47. Yamanaka K. Anodically Electrodeposited Iridium Oxide Films (AEIROF) from Alkaline Solutions for Electrochromic Display Devices. Jpn J Appl Phys [Internet]. 1989 Apr 20;28(Part 1, No. 4):632–7. Available from: https://iopscience.iop.org/article/10.1143/JJAP.28.632

48. Wu CC, Lin WC, Fu SY. The open container-used microfluidic chip using IrOx ultramicroelectrodes for the in situ measurement of extracellular acidification. Biosens Bioelectron. 2011;26(10):4191–7. Available from: http://dx.doi.org/10.1016/j.bios.2011.04.034

49. Marzouk SAM. Improved Electrodeposited Iridium Oxide pH Sensor Fabricated on Etched Titanium Substrates. Anal Chem. 2003 Mar 1;75(6):1258–66. Available from: https://pubs.acs.org/doi/10.1021/ac0261404

50. Zhao Z, Tu H, Kim EGR, Sloane BF, Xu Y. A flexible Ag/AgCl micro reference electrode based on a parylene tube structure. Sensors Actuators B Chem. 2017 Aug;247:92–7. Available from: http://dx.doi.org/10.1016/j.snb.2017.02.135

51. Anastasova S, Crewther B, Bembnowicz P, Curto V, Ip HM, Rosa B, et al. A wearable multisensing patch for continuous sweat monitoring. Biosens Bioelectron. 2017 Jul;93(June 2016):139–45. Available from: http://dx.doi.org/10.1016/j.bios.2016.09.038

52. Bitziou E, O'Hare D, Patel BA. Spatial changes in acid secretion from isolated stomach tissue using a pH-histamine sensing microarray. Analyst. 2010;135(3):482–7. Available from: http://xlink.rsc.org/?DOI=b921296e

53. Huang W, Cao H, Deb S, Chiao M, Chiao JC. A flexible pH sensor based on the iridium oxide sensing film. Sensors Actuators A Phys. 2011 Sep;169(1):1–11. Available from: http://dx.doi.org/10.1016/j.sna.2011.05.016

Annexes

Supplementary information – Materials and Methods

Parameters for CNC tools	
Stepover	0.5 mm
Stepdown	1 mm
Feed rate	20 mm/sec
Plunge rate	4 mm/sec
Spindle	6500 r.p.m

Table S1 – Parameters used for the fabrication of the moulds in the CNC machine

Supplementary information – Results and discussion

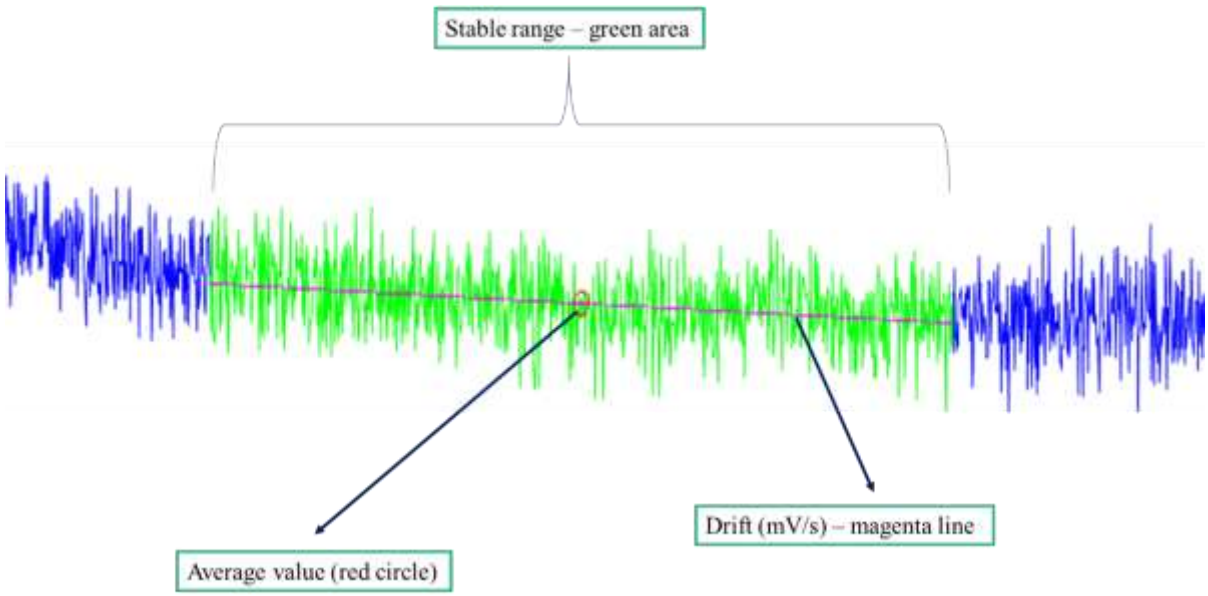

S1. Partial representation of the raw signal obtained, and the respective parameters calculated during analysis

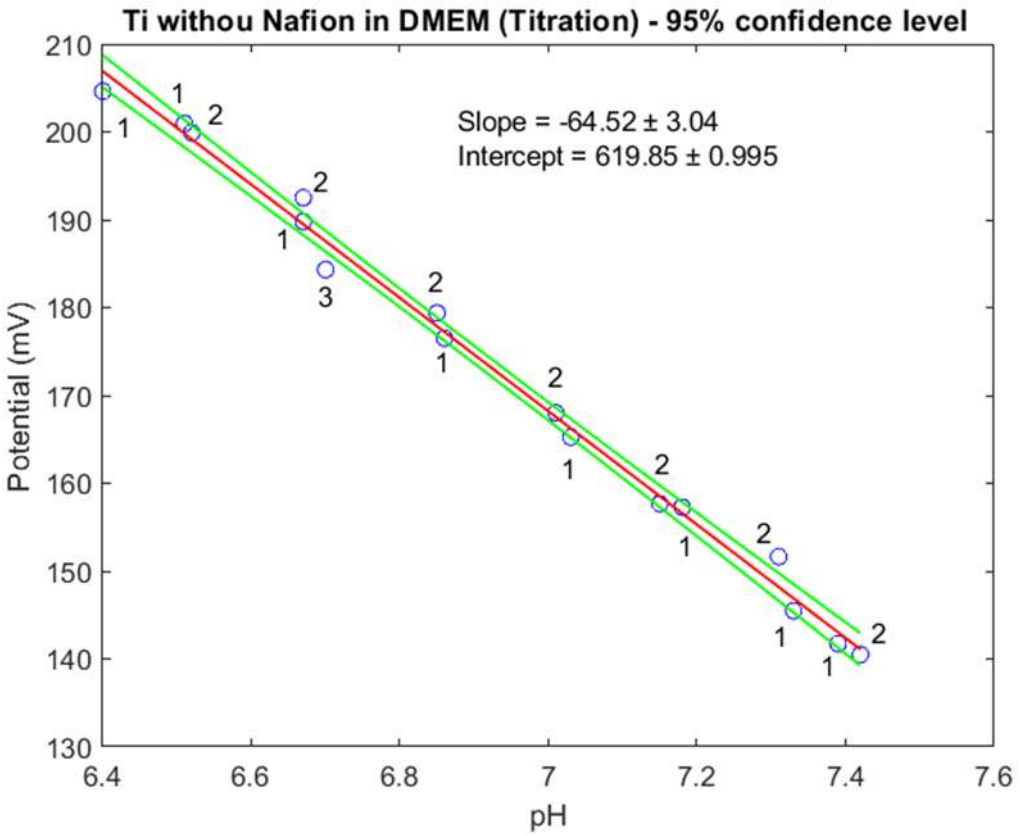

S2. Calibration (potential vs pH) determined in DMEM by the in-house-made electronic interface for titanium with IrOx coated sensor using a titration approach. 1, 2 and 3 means, adding HCl successively, followed by NaOH and going back to adding HCl, respectively